行政院國家科學委員會補助專題研究計畫 **■成果報告**
□期中進度報告

以電鍍法製作含奈米粒子之金屬微結構的熱膨脹係數及疲勞特性研究(3/3)

計畫類別：■ 個別型計畫　□ 整合型計畫
計畫編號：NSC 97 － 2221 － E － 009 － 020 － MY3
年度執行期間： 99 年 08 月 01 日至 100 年 07 月 31 日
全程執行期間： 97 年 08 月 01 日至 100 年 07 月 31 日

計畫主持人：徐文祥
共同主持人：
計畫參與人員：蔡梨暖，黃家聖，李毅家，林軒宇，鐘政涵，王澤瑋

成果報告類型(依經費核定清單規定繳交)：□精簡報告 ■完整報告

本成果報告包括以下應繳交之附件：
□赴國外出差或研習心得報告一份
□赴大陸地區出差或研習心得報告一份
■出席國際學術會議心得報告及發表之論文各一份
□國際合作研究計畫國外研究報告書一份

處理方式：除產學合作研究計畫、提升產業技術及人才培育研究計畫、列管計畫及下列情形者外，得立即公開查詢
□涉及專利或其他智慧財產權，□一年□二年後可公開查詢

執行單位：國立交通大學機械系

中 華 民 國 100 年 08 月 31 日

中文摘要：

本計畫內容在於利用低溫電鍍鎳製程，並於鍍液中加入奈米鑽石顆粒，共同沉積形成電鍍鎳基奈米複合材料，以討論奈米顆粒的添加所帶來的材料性質變化，並藉由材料性質的變化，來提升微機電元件的性能。首先，藉由不同粒子的添加，包括奈米鑽石顆粒(350nm, 125nm, 和 50nm)和二氧化矽顆粒(80nm)，可以調控複合材料熱膨脹係數與楊氏係數的提升或衰減。本實驗室是首先發現金屬奈米複材有提升熱膨脹係數特性的研究團隊，雖然複合材料楊氏係數的強化，可以藉由傳統混合法則解釋；但是對於熱膨脹係數的強化，卻無法以通常的混合法則解釋之。從 X 光繞射圖譜(XRD)的觀察，獲得複合材料中殘留應力形態與複合材料熱膨脹係數間的關係；並由穿透式電子顯微鏡(TEM)觀察奈米顆粒鑲嵌於基材中的位置，成功地解釋複合材料的殘留應力形態變化與其熱膨脹係數間的關係。其次，利用彎曲測試的方式，藉由電鍍鎳與電鍍鎳-鑽奈米複材所製成的微懸臂樑，以討論材料的疲勞行為與特性。電鍍鎳基材由於奈米鑽石顆粒的添加，使得電鍍鎳-鑽奈米複材具有較高的楊氏係數；特別是添加較小顆粒的奈米鑽石，其複材楊氏係數的提升更是顯著。根據量測的結果，當所加入的奈米鑽石粒徑從 350nm 減至 50nm，其各所形成的複材楊氏係數相較於純電鍍鎳約有 4.6%與 13.6%的提升。但是，電鍍鎳基材也因為奈米鑽石顆粒的添加，而降低材料本身的延性，進而造成複材疲勞強度的輕微衰減。然而，當所加入的奈米鑽石粒徑從 350nm 減至 50nm，奈米鑽石顆粒則可以更有效地阻止差排運動；特別是在低應力的循環負載下，電鍍鎳-鑽奈米複材具有可以和電鍍鎳相比的疲勞壽命，不會因為奈米鑽石的添加而明顯降低複材的疲勞強度。根據疲勞量測的 S-N 曲線結果，電鍍鎳的疲勞強度為 2.41GPa，而電鍍鎳-鑽奈米複材於 350nm 和 50nm 不同粒徑的添加下，其疲勞強度分別為 2.18GPa 和 2.40GPa。最後，在懸浮式微機電元件製作上，發現結構容易形成翹曲，主要為電鍍過程中生成的應力梯度所造成。藉由調整電流密度來降低鍍層的應力梯度，當電流密度由 15.3 降至 0.8 mA cm^{-2}，對於鎳與鎳-鑽奈米複材分別可降低 45%與 27%的應力梯度，可應用於製作無翹曲的微機電元件。根據楊氏係數提升的特性，將電鍍鎳-鑽奈米複材應用於梳狀共振器的製作，以 125nm 的鑽石奈米顆粒，添加濃度為 2 g L^{-1} 為例，可提升 14%共振頻率；除此之外，共振器的品質因數也隨之提升。此特性大幅提升鎳基奈米複合材料於微機電元件上的應用的可能性，特別是射頻微機電元件。

關鍵詞：奈米複材，電鍍，鎳，奈米鑽石粒子，熱膨脹係數，楊氏係數，疲勞，應力梯度，梳狀共振器，共振頻率

英文摘要：

In this project, a low-temperature electroplated Ni process with the addition of

uniformly dispersed nano-particles is proposed to deposit the Ni based nanocomposite and the variation of material properties due to the nano-particles incorporation are investigated. Basing on the material properties variation, the Ni based nanocomposite is applied in MEMS device fabrication and improves device performance. Firstly, nano-particles, including diamond (average diameter 350nm, 125nm, and 50nm) and SiO_2 (average diameter 80 nm), are incorporated and investigated for the modification of thermal expansion coefficient (CTE) and Young's modulus. Experimental results show that these material parameters can be either enhanced or deteriorated via the incorporation of different kind of nano-particles. Although the enhancement of mechanical strength can be attributed to the intrinsic characteristics of nano-particle based on the rule of mixture, the discrepancy of CTE modification can only be explained by X-ray diffraction (XRD) and transmission electron microscope (TEM) analysis on residual stress type resulting in the CTE variation. Secondly, employing the bending-test method, a fatigue characterization scheme has been performed on microsized cantilever-beam specimens made of electroplated Ni and Ni-diamond nanocomposites to investigate the related material behavior and properties thoroughly. Due to the nano-diamond incorporation in the electroplated Ni matrix, the Young's modulus reinforcement of composite can be realized especially for small particle size. According to the measurement results, Ni-diamond nanocomposites with the average particle-diameter of 350nm and 50nm can have around 4.6% and 13.6% Young's modulus enhancement than that of pure electroplated Ni, respectively. Meanwhile, the results also show that Ni-diamond nanocomposite has slightly smaller fatigue strength than that of pure electroplated Ni due to the ductility reduction resulted by the nano-diamonds. Nevertheless, once incorporated diamond particle size is reduced from 350nm to 50nm, it has been found that the nano-diamond particles can effectively hinder dislocation motion so that the fatigue lifetime of Ni-diamond nanocomposite can be comparable with that of pure electroplated Ni without sacrificing its fatigue strength, especially in low stress cycling regime. According to the test results of fatigue lifetime in terms of *S-N* curve, the values of fatigue strength are obtained as 2.41GPa, 2.18GPa, and 2.40GPa for electroplated Ni and Ni-diamond nanocomposites with the average particle-diameter of 350nm and 50nm, respectively. Finally, the stress gradient caused curl suspended structure is eliminated by the reduction of plating current density. By lowering the plating current density from 15.3 to 0.8 mA cm^{-2}, about 45% and 27% of the stress gradient reduction in the Ni and Ni-diamond nanocomposite films can be realized and utilized for MEMS resonator fabrication without having structural warpage. Experimental result shows that the performance of the Ni-diamond nanocomposite comb resonator with 125 nm nano diamond

particles (2 g L^{-1}) can be enhanced 14% resonant frequency. Furthermore, the quality factor also increases. The property enhancements have led such electroplated Ni-based nanocomposite films for more MEMS applications, especially in RF MEMS.

Key words：Nanocomposite, Electroplating, Ni, Nano diamond particle, CTE, Young's modulus, Fatigue, Stress gradient, comb resonator, resonant frequency

報告內容：

Part I

1. Introduction

Electro-deposition has been a manifest process technique for cost-effective MEMS (microelectromechanical systems) fabrication. This technique provides several advantages including flexible material choice, low temperature CMOS compatible process, and high manufacturing throughput. For instance, electroplated Ni can have comparable mechanical properties with poly-silicon but even lower electrical and thermal resistivity, lower processing temperature, and higher deposition rate. Since 1988, lots of research works have been done in the electroplated Ni for MEMS fabrication and application [1-6].

Recently, the nanotechnology has further advanced the electroplating technique in terms of material property enhancement for various MEMS applications. Combining with the strengthening and size effects originated from the incorporation of well distributed nano-particles like diamond, SiC, Al_2O_3, and Si_3N_4 [7-12], electroplated metal-nanocomposite can exhibit superior physical properties beyond the limits of intrinsic metal. Teh *et al.* [10] have shown Ni-based nanocomposite synthesis method for MEMS devices fabrication. Huang *et al.* [11] have demonstrated a low power magnetic microactuator using Cu-Ni nanocomposite as the inductive coil material. For electro-thermal microactuator application, Tsai *et al.* [12] have shown that the microactuator made of Ni-diamond nanocomposite can reduce 73% power requirement of pure Ni one needed for the same output displacement of 3 μm and enlarge the reversible displacement range from 1.8 to 3 μm, simultaneously. The performance enhancements are resulted by the augment of coefficient of thermal expansion (CTE) and hardness of Ni via the nano-diamond particle incorporation. Thus, employing the nanocomposites synthesized by electro-deposition process for MEMS fabrication has revealed its excellent prospect.

This presented work will investigate nano-particle size and composite effects on the modification of material properties of electroplated Ni. Via the understanding of the correlation, such a Ni-based nanocomposite provides an alternative research direction in the future development of MEMS fabrication using nanocomposites.

2. Fabrication

In the prior work [12], cantilever beams made of electroplated Ni or Ni-diamond nanocomposite were utilized for characterizing the CTE property. By measuring the elongation of cantilever beam in a heated chamber with temperature control, the CTE of material can be obtained. The cantilevers are all fabricated using the electroplating Ni process with the addition of uniformly dispersed nano-particles. Different sizes of nano-diamond particles, which are 350 nm, 125 nm, and 50 nm in average diameter respectively, will be added into a sulfuric based Ni plating bath for the investigation of size effect and 80 nm in average diameter of nano-SiO_2 particle is chosen here for comparison purpose, which will be discussed later. The amount of nano-particle incorporation in Ni matrix is controlled using different plating bath with different particle concentration. In the experiment, the Ni-diamond and Ni-SiO_2 nanocomposites are synthesized in different plating solutions, which have the concentration of the nano-diamond particles ranging from 0 to 2 g/L and the concentration of the nano-SiO_2 particles ranging from 0 to 0.036 g/L, respectively. Table 1 shows the detail plating bath compositions, conditions, and the concentration of nano-particles in the bath.

Table 1. Plating bath conditions of Ni-diamond and Ni-SiO_2 nanocomposite.

Ni-diamond nanocomposite	
Batch:	
Nickel sulfamate (g/L)	400
Nickel chloride (g/L)	5
Boric acid (g/L)	40
Wetting agent (c.c.)	5
Concentration of diamond nano-particle (g/L)	2, 1, 0.5
Average diameter of diamond nano-particle (nm)	350, 125, 50
pH	4.1 ~ 4.3
Current density (mA/cm^2)	10
Temperature (°C)	50
Ni-SiO_2 nanocomposite	
Batch:	
Nickel sulfamate (g/L)	400
Nickel chloride (g/L)	5
Boric acid (g/L)	40
Wetting agent (c.c.)	5

Concentration of SiO_2 nano-particle (g/L)	0.008, 0.018, 0.036
Average diameter of SiO_2 nano-particle (nm)	80
pH	4.1 ~ 4.3
Current density (mA/cm^2)	10
Temperature (°C)	50

As shown in Fig. 1, all device fabrication starts with a silicon wafer with 0.5 μm thick SiO_2 deposition followed by 2 μm thick FH-6400 photoresist (PR) coating. The PR is then patterned and hard baked as sacrificial layer. Then, a layer of 1000 Å Cu/100 Å Ti is sputtered as plating seed layer followed by another 8 μm thick AZP-4620 PR coating that is patterned as an electroplating mold. After that, Ni or Ni-based nanocomposite films are electroplated at 50 °C to form the cantilever beams. Finally, the fabricated cantilever beams are released after stripping the sacrificial layer by acetone solution. Fig. 2 shows the SEM micrographs of as-fabricated cantilever beams made of Ni-diamond and Ni-SiO_2 nanocomposites, respectively.

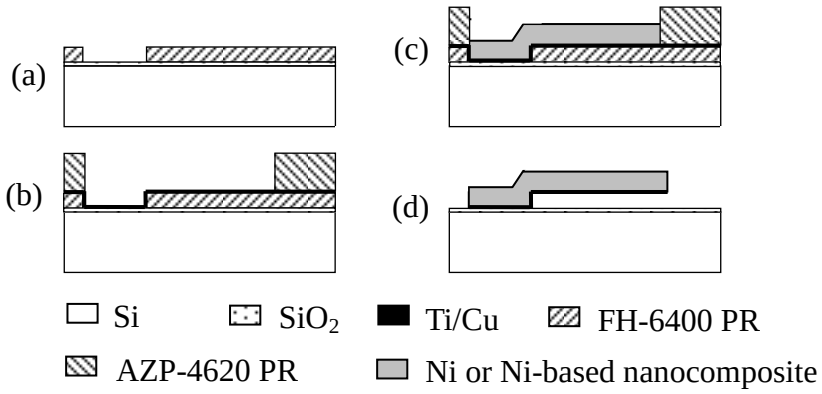

Fig. 1. Fabrication process of Ni-based cantilever beam.

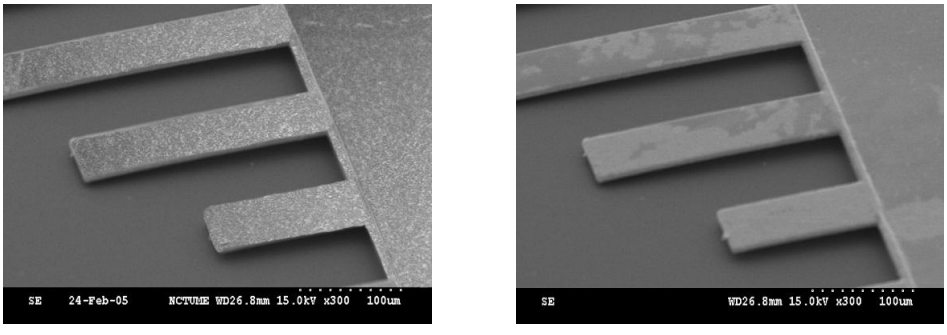

(a) **(b)**

Fig. 2. SEM pictures of fabricated cantilever beams made of: (a) Ni-diamond (average diameter 50 nm, 2 g/L), and (b) Ni-SiO_2 (average diameter 80 nm, 0.036 g/L) nanocomposites.

3. Results

3.1 Process characterizations

The plating process is characterized via the analysis of elemental analyzer (EA). The weight fractions of nano-diamonds in the Ni matrix with different plating concentrations are measured by EA as shown in Fig. 3. The volume fractions of nano-diamonds in the matrixes are calculated based on the density of nickel (8.908 g/cm^3) and the density of diamond powder (3.51 g/cm^3). The analyses show that the concentrations of the embedded nano-diamonds increase with the amount of the diamond powders being added into the plating bath. Besides, the smaller the nano-diamonds are put into the plating bath, the larger the volume fraction of the nano-diamonds will be incorporated in the Ni matrix. In contrast, because the EA cannot be used for the analysis of incorporated SiO_2 concentration in the Ni-SiO_2 nanocomposite system, the energy dispersive spectrum (EDS) is then used to examine the existence of SiO_2. Fig. 4 shows the spectrums of two samples which are pure Ni and the Ni-SiO_2 nanocomposite plated in the bath with the concentration of 0.036 g/L SiO_2. As compared, the nanocomposite has not only O peak but also Si peak with higher intensity than the pure Ni does, which could be attributed to the existence of incorporated SiO_2. Because there is no obvious spectrum difference between the pure Ni and the nanocomposites plated in the baths with 0.008 and 0.018 g/L SiO_2, respectively, it is suggested that the concentrations of the embedded nano-SiO_2 particles also increase with the amount of the diamond powders being added into the plating bath.

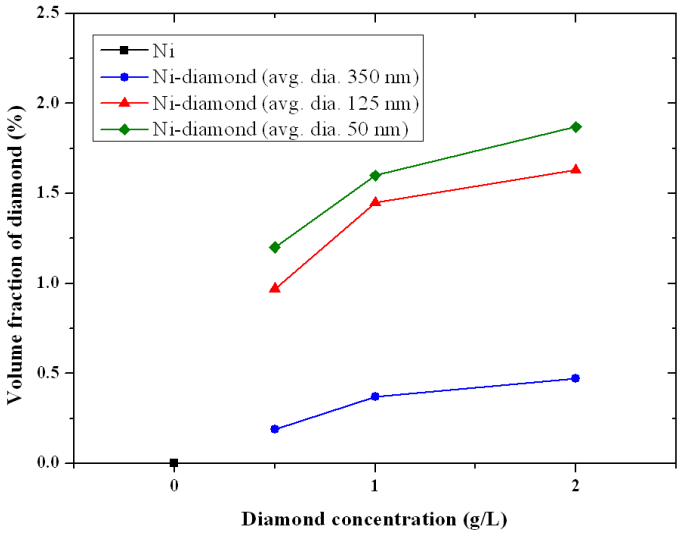

Fig. 3. Volume fractions of nano-diamonds in the Ni matrixes of different concentrations and average diameters of nano-diamond particles.

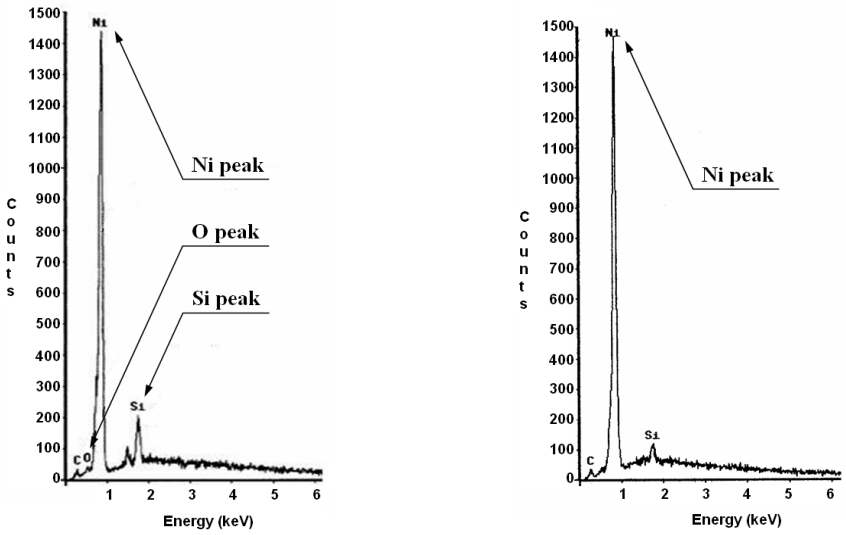

(a) **(b)**

Fig. 4**.** EDS spectrums of (a) Ni-SiO_2 nanocomposite (0.036 g/L) and (b) pure electroplated nickel.

3.2 CTE and Young's modulus characterizations

In the experiment, material CTE properties are investigated by measuring the elongation of cantilever beams made of electroplated Ni or Ni-based nanocomposite in a heating chamber at 400 °C. Fig. 5 compares the CTE properties of pure electroplated Ni and Ni-diamond nanocomposites with different concentrations and sizes of incorporated particles. Experiment results show that the CTE of Ni-diamond nanocomposites is higher than that of pure electroplated Ni (23×10^{-6}/°C as measured) and increases with the concentration of incorporated nano-diamond. For the nanocomposites plated in a bath with 125 nm nano-diamonds, the CTE values increase from the 34.5×10^{-6}/°C to 40.2×10^{-6}/°C while the nano-diamond concentration in the bath increase from 1 to 2 g/L. Furthermore, more than two times enlargement of CTE value of Ni-diamond nanocomposite in average diameter 350 nm with the concentration of 2 g/L than pure electroplated Ni. However, with the reduction of the particle size of nano-diamond, the CTE values are found to decrease from 50×10^{-6}/°C of the composite synthesized with the nano-diamonds of average diameter 350 nm down to 38×10^{-6}/°C of that with the nano-diamonds of average diameter 50 nm. In contrast to nano-diamond particle, the CTE value decreases with the concentration of SiO_2 nano-particles in the plating bath from 22×10^{-6}/°C of 0.008 g/L to 18×10^{-6}/°C of 0.036 g/L.

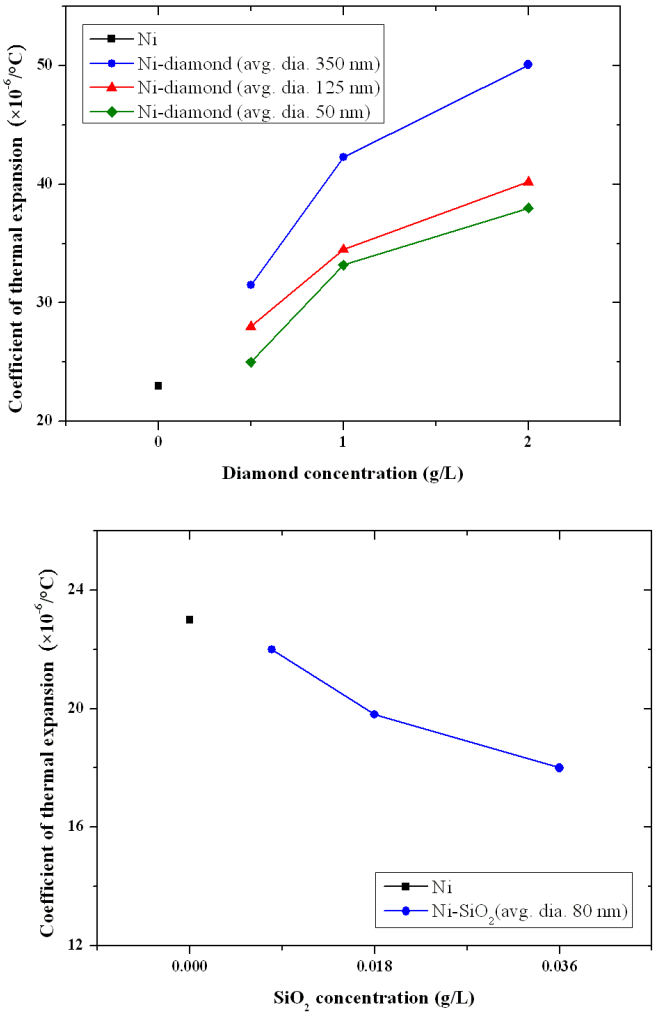

(a) (b)

Fig. 5. Comparison of CTE properties (at 400 °C) between pure electroplated Ni and Ni-based nanocomposites: (a) Ni-diamond and (b) Ni-SiO_2 with different particle sizes and concentrations.

In this work, Young's modulus is measured by means of a nanoindentation test using a Nano Indentor® XP from MTS Systems Corporation. Fig. 6 compares the Young's modulus of pure electroplated Ni and Ni-based nanocomposites, respectively, with different particle sizes and concentrations. The Young's modulus of Ni-diamond nanocomposites increases with the increase of diamond concentration and the decrease of nano-particle size. For a Ni-diamond nanocomposite plated with nano-diamond concentration of 2 g/L and particle size of 50 nm, the Young's modulus (~236.7 GPa, as measured) can be enhanced up to 1.24 times larger than that of pure electroplated Ni (~190.6 GPa, as measured). Because diamond has a higher Young's modulus (~1100 GPa [13]) than that of pure electroplated Ni, it can be expected that the material of Ni-diamond nanocomposite will have a higher Young's modulus,

based on the rules of mixture [14]. It also explains that the modulus of Ni-SiO_2 nanocomposite decreases with the increase of SiO_2 concentration due to the lower Young's modulus of SiO_2 particle (~70 GPa [15]) relative to pure electroplated Ni. Being with the SiO_2 particle concentration of 0.036 g/L, the Young's modulus of the Ni-SiO_2 nanocomposite has been lowered down to 180 GPa.

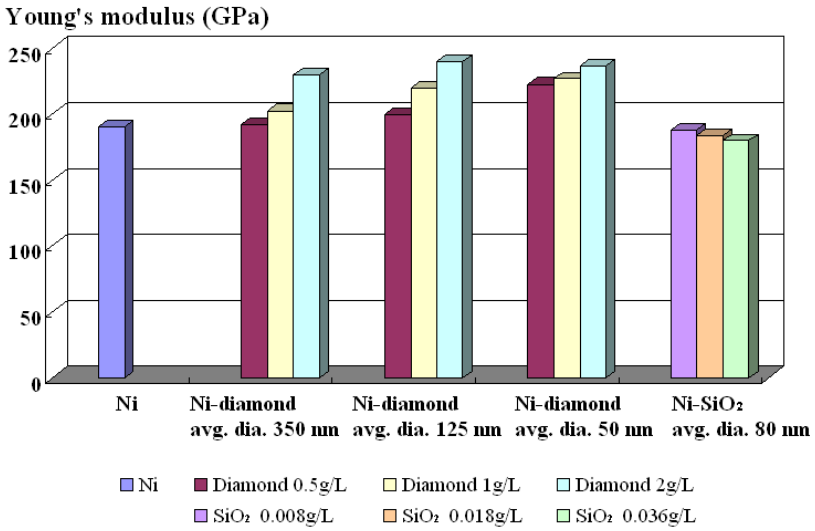

Fig. 6. Comparison of Young's modulus between pure electroplated Ni and Ni-based nanocomposites including Ni-diamond and Ni-SiO_2 with different particle sizes and concentrations.

3.3 Nanocomposite effects

As mentioned, although the incorporation of diamond particles in Ni matrix can augment CTE and Young's modulus parameters, the simple rule of mixture used for explaining conventional composite material's behavior [16-18] could not well qualitatively and quantitatively explain the discrepancy between the model prediction and the measurement results.

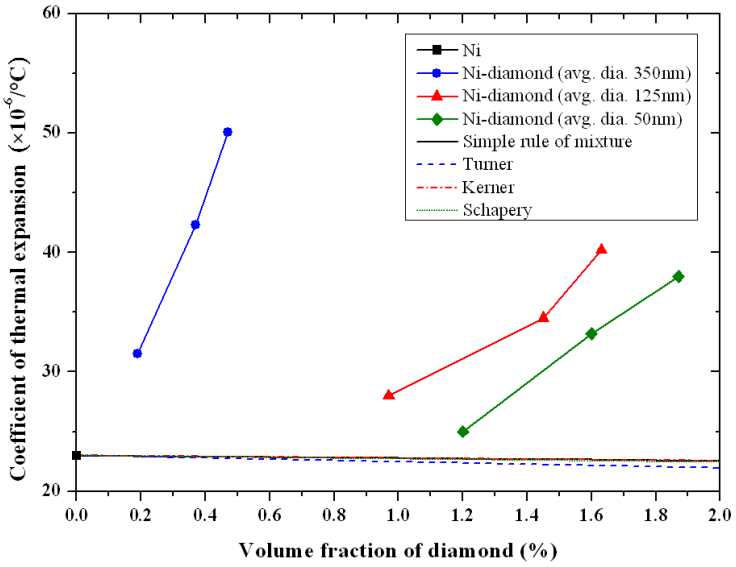

Fig. 7. Comparison of CTE between experimental data and model predictions of Ni-diamond nanocomposites.

Fig. 7, for instance, shows the CTE of Ni and Ni-diamond nanocomposites with For the CTE value of Ni-diamond nanocomposite (22.9 $\times 10^{-6}$/°C) from [16, 17]:

$$\alpha_c = V_m \alpha_m + V_p \alpha_p \quad (1)$$

where α_c, α_m and α_p are CTEs of the composite, matrix (α_{Ni}: 23 $\times 10^{-6}$/°C, as measured) and particle ($\alpha_{diamond}$: 0.9 $\times 10^{-6}$/°C [19]), respectively. V_p is the volume fraction of the particle — an approximated 0.47% of nano-diamond particles occupied the Ni matrix. Although the CTE property of Ni-diamond nanocomposite doesn't conform to the simple rule of mixture, this discrepancy can be explained and further investigated by X-ray diffraction (XRD) analysis and transmission electron microscope (TEM) of the crystalline texture variation which result by the incorporation of nano-diamond particles. The correlation between nano-diamond particle effect and CTE property is demonstrated for electroplated Ni-diamond nanocomposite from XRD and TEM analysis.

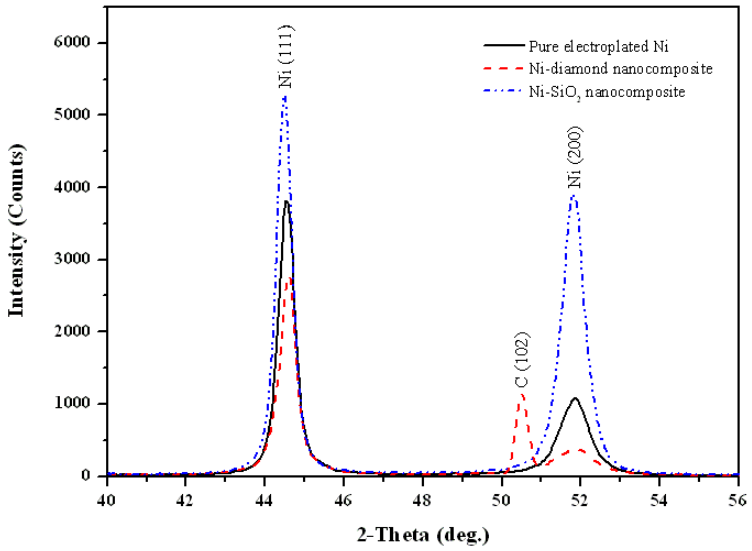

Fig. 8. The XRD patterns at room temperature for the as-fabricated pure Ni, Ni-diamond, and Ni-SiO_2 nanocomposites.

Fig. 8 shows the XRD patterns at room temperature for the as-fabricated pure Ni and Ni-based nanocomposites, respectively. The face-centered-cubic (FCC) texture of electroplated pure Ni and Ni-based nanocomposites have been observed with (111) preferred orientation of grain structure. From the comparison of peak-position between electroplated pure Ni and Ni-based nanocomposite, the residual stress types of Ni-diamond and Ni-SiO_2 nanocomposites can be determined easily by the variation of the lattice spacing as the following equation [20]:

$$\varepsilon = \frac{d' - d_0}{d_0} \quad (2)$$

where d_0 is the lattice spacing of stress-free material, and d' is that for strained material. If we assume that pure electroplated Ni is stress-free material, and Ni-diamond and Ni-SiO_2 nanocomposites are strained materials. The strains of Ni-diamond and Ni-SiO_2 nanocomposites can be determined as -0.15% and 0.09%, respectively, from Eq. (2). Meanwhile, it can be obtained that the incorporation of nano-diamond particles in Ni causes compressive strain in nanocomposite, and the incorporation of SiO_2 nano-particles in Ni causes tensile strain in nanocomposite. Thus, residual compressive stress type is observed in Ni-diamond nanocomposite with CTE enhancement. Oppositely, residual tensile stress type is observed in Ni-SiO_2 nanocomposite with CTE diminution. This result can also be found from the past research [21]. To further investigate the residual stress types resulted by the co-deposition of nano-particles with Ni, TEM analysis of crystalline texture is performed.

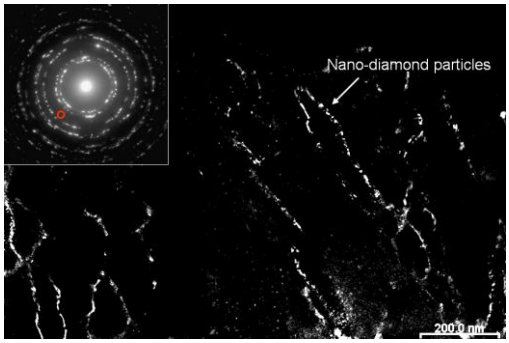

(a)

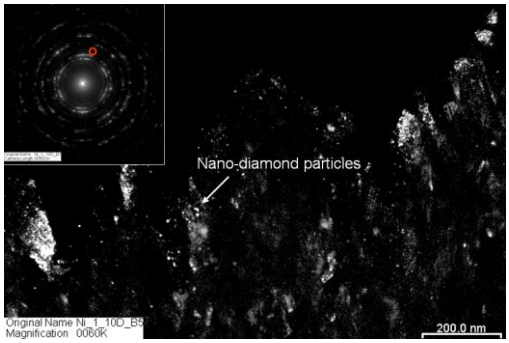

(b)

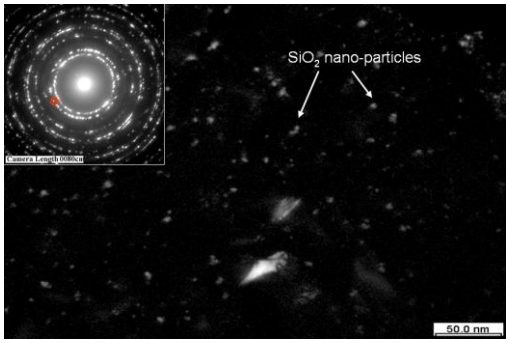

(c)

Fig. 9. Dark field TEM images of electroplated (a) Ni-diamond nanocomposite (average diameter 350 nm, 2 g/L, 0.47% v/v), (b) Ni-diamond nanocomposite (average diameter 50 nm, 2 g/L, 1.87% v/v), and (c) Ni-SiO2 nanocomposite (average diameter 80 nm, 0.036 g/L).

Fig. 9 shows the dark field TEM images of nano-diamond particles and nano-SiO_2 particles distribute in the Ni matrix. In this observation scale of Ni-diamond nanocomposite, we found that nano-diamond particles have different distribution in Ni matrix with different adding particle size in the plating bath. In Fig. 9a, the nano-diamond particles distribute in the grain boundary regions of the Ni matrix as the adding particle size is 350 nm in average diameter inside plating bath. However, with size the reduction of the adding diamond particles from 350 nm to 50 nm in plating bath, the distribution of nano-diamond particles migrate from grain

boundary regions into Ni grains as shown in Fig. 9b. Similarly, the intra-distribution of nano-particles in Ni grains is also observed on Ni-SiO_2 nanocomposite in Fig. 9c. As carried before, the CTE value of Ni-based nanocomposite comparing to Ni matrix would decrease due to the size reduction of adding diamond and different particle type like SiO_2. From the TEM analysis of crystalline texture in Fig. 9b and 9c, it is observed that the common point between diamond and SiO_2 nano-particles is intra-grain distribution. This intra-grain distribution of nano-particles will cause the residual tensile stresses inside Ni grains which decrease the CTE value of Ni-based nanocomposite. Oppositely, as shown in TEM analysis of Fig. 9a the inter-grain distribution of nano-particles will cause the residual compressive stresses inside Ni grains which increase the CTE value of Ni-based nanocomposite.

4. Conclusions

This paper reveals several new composite effects on the material property modification, especially on CTE, based on the incorporation of diamond or SiO_2 nano-particles into Ni matrix by low-temperature electrodeposited process. Through a simple composite-plating process, material properties can be modified easily in the expected way. In addition, electrodeposited Ni-based nanocomposites are compatibility with MEMS and CMOS fabrication technologies via a one-step, selective on-chip deposition process at low temperatures. These Ni-based nanocomposites are not only attractive for performance modification on CTE and Young's modulus but also may provide an alternative direction in the development of other MEMS devices using nanocomposites.

Reference

[1] W. Ehrfeld, F. Götze, D. Münchmeyer, W. Schelb, and D. Schmidt, "LIGA process: Sensor construction techniques via X-ray lithography," in *Technical Digest, IEEE Solid-State Sensor and Actuator Workshop*, Hilton Head, SC, pp. 1–4, 1988.

[2] S. Furukawa, S. Roy, H. Miyajima, Y. Uenishi, and M. Mehregany, "Nickel surface micromachning," in *Proc. IEEE Microstructures and Microfabricated Systems*, San Francisco, CA, pp. 38–46, 1994.

[3] Q. Shi, S.C. Chang, M.W. Putty, and D.B. Hicks, "Characterization of electroformed nickel microstructures," in *Proc. SPIE*, vol. 2639, pp. 191–199, 1995.

[4] P.M. Zavracky, S. Majumber, and E. McGruer, "Micromechanical switches fabricated using nickel surface micromachining," *J. Microelectromech. Syst.*, vol. 6, no. 1, pp. 3–9, 1997.

[5] C.P. Hsu, W.C. Tai, and W. Hsu, "Design and analysis of an electrothermally

driven long-stretch micro drive with cascaded structure," in *Proc. ASME International Mechanical Engineering Congress & Exposition*, New Orleans, Louisiana, 2002.

[6] K. Kataoka, S. Kawamura, T. Itoh, K. Ishikawa, H. Honma, and T. Suga, "Electroplating Ni micro-cantilevers for low contact-force IC probing, *Sens. Actuators A*, vol. 103, pp. 116–121, 2003.

[7] A.F. Zimmerman, G. Palumbo, K.T. Aust, and U. Erb, "Mechanical properties of nickel silicon carbide nanocomposites," *Mater. Sci. Eng. A*, vol. 328, pp. 137–146, 2002.

[8] J. Steinbach and H. Ferkel, "Nanostructured Ni-Al_2O_3 films prepared by DC and pulsed DC electroplating," *Scripta Mater.*, vol. 44, pp. 1813–1816, 2001.

[9] X. Li and Z. Li, "Nano-sized Si_3N_4 reinforced NiFe nanocomposites by electroplating," *Mater. Sci. Eng. A*, vol. 358, pp. 107–113, 2003.

[10] K.S. Teh, Y.T. Cheng, and L. Lin, "MEMS fabrication based on nickel-nanocomposite: film deposition and characterization," *J. Micromech. Microeng.*, vol. 15, pp. 2205–2215, 2005.

[11] Y.W. Huang, T.Y. Chao, C.C. Chen, and Y.T. Cheng, "Power consumption reduction scheme of magnetic microactuation using electroplated Cu–Ni nanocomposite," *Appl. Phys. Lett.*, vol. 90, 244105 , 2007.

[12] L.N. Tsai, G.R. Shen, Y.T. Cheng, and W. Hsu, "Performance improvement of an electrothermal microactuator fabricated using Ni-diamond nanocomposite," *J. Microelectromech. Syst.*, vol. 15, pp. 149–158, 2006.

[13] D. Schneider and M.D. Tucker, "Non-destructive characterization and evaluation of thin films by laser-induced ultrasonic surface waves," *Thin Solid Films*, vol. 290-291, pp. 305–311, 1996.

[14] A.J. Owen and I. Koller, "A note on the Young's modulus of isotropic two-component materials," *Polymer*, vol. 37, pp. 527–530, 1996

[15] M.T. Kim, "Influence of substrates on the elastic reaction of films for the microindentation tests," *Thin Solid Films*, vol. 283, pp. 12–16, 1996.

[16] A.A. Fahmy and A.N. Ragai, "Thermal-expansion behavior of two-phase solids," *J. Appl. Phys.*, vol. 41, pp.5108–5111, 1970.

[17] S. Lemieus, S. Elomari, J.A. Nemes, and M.D. Skibo, "Thermal expansion of isotropic Duralcan metal–matrix composites," *J. Mater. Sci.*, vol. 33, pp. 4381–4387, 1998

[18] C.L. Hsieh and W.H. Tuan, "Elastic and thermal expansion behavior of two-phase composites," *Mater. Sci. Eng. A*, vol. 425, pp. 349–360, 2006.

[19] D.D.L. Chung, "Materials for thermal conduction," *Appl. Therm. Eng.*, vol. 21, pp. 1593–1605, 2001.

[20] K.Tanaka and Y. Akiniwa, “Diffraction measurements of residual macrostress and microstress using X-rays, synchrotron and neutrons,” *JSME Int. J. Ser. A*, vol. 47, pp. 252-263, 2004.
[21] W. Fang and C.Y. Lo, “On the thermal expansion coefficients of thin films,” *Sensor. Actuat. A*, vol. 84, pp.310-314, 2000.

Part II

1. Introduction

Previously, we have reported that the electrolytic Ni matrix with the incorporation of nano-diamonds could exhibit higher Young’s modulus and coefficient of thermal expansion (CTE) [1, 2]. Via the property modification based on the nanocomposite effects, MEMS devices made of the nanocomposite can have superior performance. For example, electro-thermal microactuator made of the nanocomposite can have lower power, larger output force, and ultimate elongation in comparison with the one made of pure electroplated Ni due to the Young’s modulus and CTE enhancement of structural material. Micro-resonator made of the nanocomposite can increase its resonance frequency and make itself practical for electro-mechanical signal processing application to RF system [3]. Therefore, the investigation of fatigue property of the electroplated Ni-diamond nanocomposite is essential for the potential application in the fabrication of microelectromechanical systems (MEMS), where moving components are subjected to cyclic load.

To date, a variety of testing methods have been proposed for the fatigue characterization of microsized material. Among these methods, tension and bending tests are two popular testing schemes. Tension method [4, 5] can extract Young’s modulus and fracture strength directly from the measured stress-stain curve. However, once the sample becomes very small only with several millimeters [6], the setup requirements for gripping, aligning, and pulling a tested sample become stringent to the method. In comparison with the tension method, bending method [7, 8] can be free of the issues raised by sample gripping and alignment. Furthermore, bending test only requires smaller loading force than that of tension test to yield tested sample with a deformation large enough for accurate measurement, which makes the method suitable for thin film characterization. Thus, in this study, a fatigue characterization scheme based on the bending-test design is proposed and utilized for the property investigation of the Ni-based nanocomposite in terms of Young’s modulus, fatigue life, fatigue strength, and fracture mechanism.

2. Experimental setup and test sample design

Fig. 1 shows the scheme of the bending-fatigue test where microsized

cantilever-beam specimen is tested in a displacement-control mode. A tungsten micro-probe is controlled by the test machine to cyclically exert a loading force on the free-end of cantilever beam with a fixed vertical displacement [9]. Before sample testing, the contact monitoring between micro-probe and microsized cantilever-beam specimen is detected by the load cell underneath the tested specimen. Through the load cell fixed on a precise x-y table and the charge-coupled device (CCD) system, the micro-probe can accurately be placed on the right load-position of microsized cantilever-beam specimen. In this fatigue test machine, the resolutions of load cell and displacement actuation can be controlled at 0.1mN and 0.1μm, respectively. Fig. 2 shows the scheme of microsized cantilever-beam specimen for bending-fatigue test. A contact hole is introduced in the specimen design as the load-position to fix the micro-probe with specimen for preventing the probe-tip from gliding along the beam during the test [10]. The contact hole, 15μm in diameter, is located on the center line of cantilever beam with 130μm from the root of the beam and 50μm from the free-end. The designed width (*w*) and thickness (*t*) of the microsized cantilever-beam specimen are fixed at 50μm and 15μm, respectively.

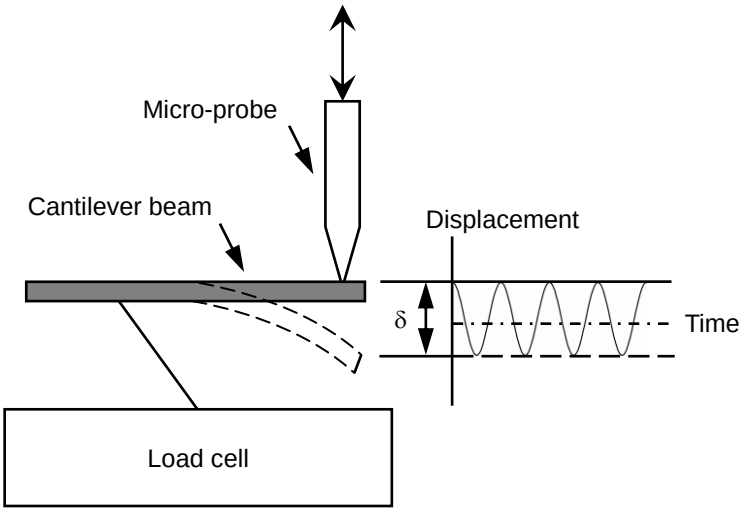

Fig. 1. Schematic set-up of the bending-fatigue test for microsized cantilever-beam specimen.

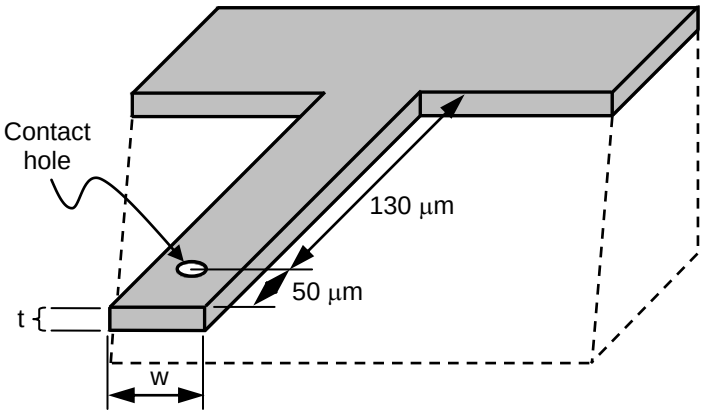

Fig. 2. Illustration of microsized cantilever-beam specimen.

The microsized cantilever-beam specimens are fabricated on a silicon substrate as shown in Fig. 3. Initially, the Ti adhesion layer (200Å thick) and Cu seed layer (1000Å thick) are sputtered respectively onto the cleaned silicon wafer. Then, the 20μm thick AZP-4620 photoresister (PR) is spin coated and patterned to form the plating molds of microsized cantilever-beam specimens (Fig. 3(a)). Subsequently, the electroplated Ni-based material is deposited to construct the microsized cantilever-beam specimens (Fig. 3(b)). Table 1 shows the plating bath conditions of electroplated Ni-based materials of pure Ni and Ni-diamond nanocomposites. For the composite-plating of Ni-diamond nanocomposites which are different from pure electroplated Ni, the nano-diamond particles with the average particle-diameters of 350nm and 50nm are added respectively into the different plating baths of sulfuric-based Ni for the co-deposition. And the concentrations of nano-diamond particles in plating baths are all kept at 2g/L. Finally, the fabricated cantilever-beam specimens are released after stripping the plating molds by acetone solution (Fig. 3(c)), which is followed by the removal of silicon underneath using KOH solution (Fig. 3(d)).

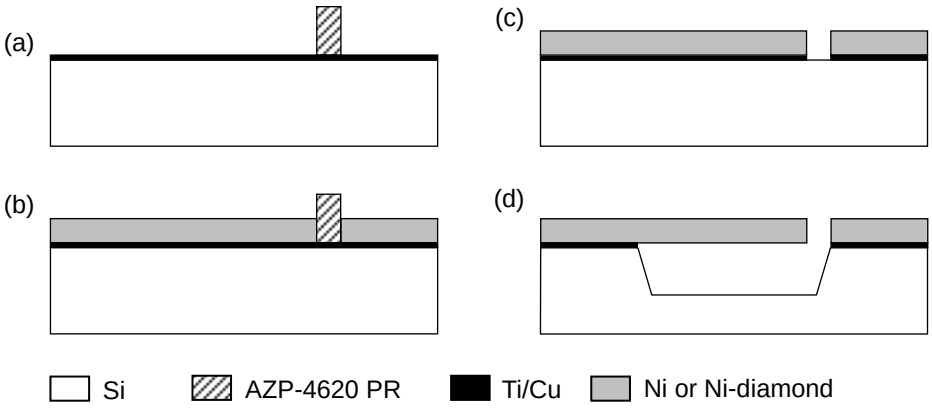

Fig. 3. Fabrication process of microsized cantilever-beam specimen.

Table 1. Plating bath conditions of Ni-based materials for microsized cantilever-beam specimens.

Ni	
Batch	
Nickel sulfamate (g/L)	400
Nickel chloride (g/L)	5
Boric acid (g/L)	40
Wetting agent (c.c.)	5
pH	4.1–4.3
Current density (mA/cm^2)	10
Temperature (°C)	50
Ni-diamond nanocomposites	
Batch	
Nickel sulfamate (g/L)	400
Nickel chloride (g/L)	5
Boric acid (g/L)	40
Wetting agent (c.c.)	5
Concentration of diamond nanoparticles (g/L)	2
Average diameter of diamond nanoparticle (nm)	50, 350
pH	4.1–4.3
Current density (mA/cm^2)	10
Temperature (°C)	50

Fig. 4 shows the scanning electron microscope (SEM) pictures of as-fabricated cantilever-beam specimens made of electroplated Ni and Ni-diamond nanocomposites for the bending-fatigue test, respectively. According to the elemental analyzer (EA) measurement of the synthesis of Ni-diamond nanocomposites, the diamond content of the corresponding nanocomposite films with the average particle-diameters of 350nm and 50nm are 0.14% and 0.16% in weight fraction, respectively. Furthermore, according to the calculation based on the density of electroplated Ni (8908kg/m^3 [1]) and diamond (3510kg/m^3 [1]), the diamond content of Ni-diamond nanocomposite films with the average particle-diameters of 350nm and 50nm are 0.35% and 0.41% in volume fraction, respectively.

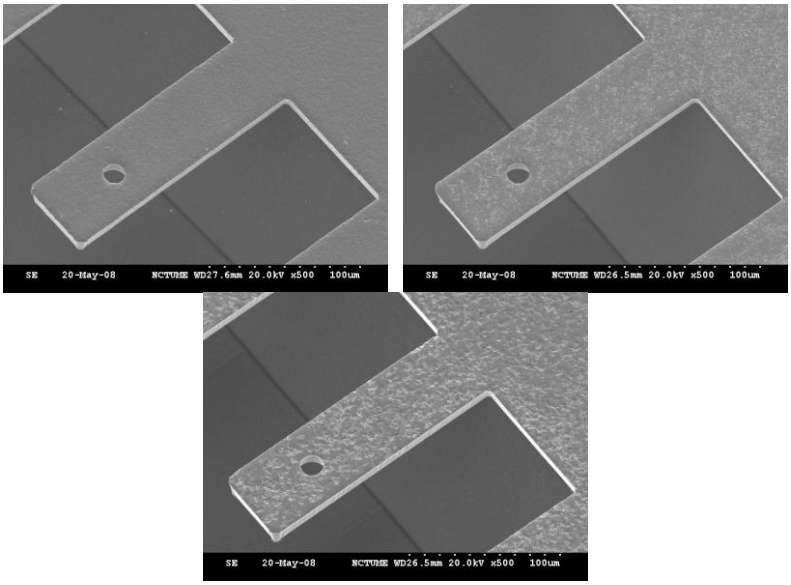

(a) (b) (c)

Fig. 4. SEM pictures of as-electroplated cantilever-beam specimens made of: (a) Ni; (b) Ni-diamond nanocomposite with average particle-diameter of 350nm; (c) Ni-diamond nanocomposite with average particle-diameter of 50nm.

3. Measurements and results

3.1 Static bending test

Before the test of fatigue lifetime, a static bending test is performed on as-fabricated cantilever nanocomposite beams to determine fatigue-test conditions. Firstly, a tungsten probe tip connected to the test machine is precisely placed at the contact hole of the beams, and the loading force applied by the probe to the beam is measured by a load cell connected to the computer. The tested beam is then gradually deflected by the probe-tip from 0 to 50μm with a displacement step of 2μm. Thus, the loading force versus corresponding displacement can be recorded by the load cell as shown in Fig. 5, which is force-displacement (F-δ) curve. As the fatigue-test condition in this study, the maximum displacement loading (δ_{max}) range is determined by the proportional limit of F-δ curve. In this range, the force is proportional to the specimen defection. As shown in Fig. 5, the δ_{max} are determined as 18μm, 22μm, and 18μm for the electroplated Ni beam and the Ni-diamond nanocomposite beams where the average particle-diameters of nano-diamonds are 350nm and 50nm, respectively.

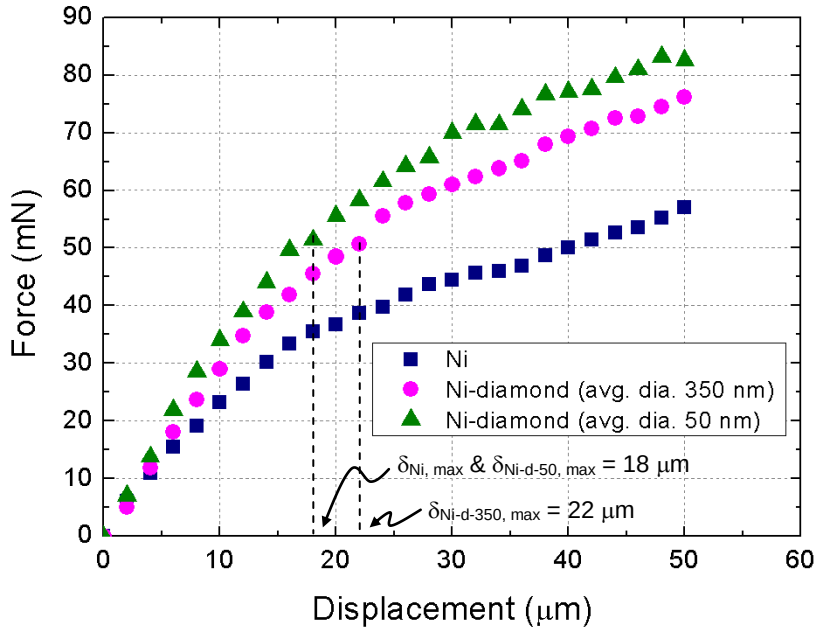

Fig. 5. Force-displacement (*F*-δ) curve of microsized cantilever-beam specimens made of the electroplated Ni and Ni-diamond nanocomposites from the static bending tests.

3.2 Young's modulus measurement

According to Fig. 5, the slope of *F*-δ curve also indicates that the incorporation of nano-diamonds in Ni matrix can enhance the stiffness (force/displacement) of specimen than that of pure electroplated Ni. Using these stiffness data, the Young's modulus of specimen material can be extracted from the following cantilever-beam equation:

$$E = \frac{L^3}{3I} \cdot \frac{F}{\delta} \quad (1)$$

where L is the length from the beam-root to the load-position, and I is the moment of inertia. Because the equation is only built for idea case without considering actual boundary conditions like quarter-plane and undercut [11] which usually occur in wet-etching process, the extracted Young's modulus becomes unreasonable. In order to solve this problem, commercial finite-element-analysis (FEA) software, ANSYS, is employed to estimate the accurate Young's modulus of the tested samples. Through the construction of *F*-δ curve analyzed by ANSYS based on the actual parameters of beam size and undercut size, the stiffness can be simulated and compared with the experimental stiffness calculated from data in Fig. 5. Once the analytical data is matched with the experimental one, the corresponding of Young's modulus values can be obtained as 156.9GPa, 165.9GPa, and 178.2GPa for the

electroplated Ni and Ni-diamond nanocomposites with the average particle-diameter of 350nm and 50nm, respectively. To further examine the derived Young's modulus values from FEA, the analyzed Young's modulus values of the electroplated films and the resonant frequencies of the tested beams are also compared with the data measured by nanoindenter [12] and LDV resonant frequency measurement method [13], respectively. Table 2 lists the measured Young's modulus values from nanoindenter and resonance methods which well agree with the results of FEA. It is noted that Ni-diamond nanocomposites with the average particle-diameters of 350nm and 50nm both have Young's modulus values which are about 4.6% and 13.6% larger than that of pure electroplated Ni, respectively.

Table 2. Young's modulus values of the electroplated films of Ni and Ni-diamond nanocomposites measured by FEA, nanoindenter, and resonance methods.

	FEA	**Nanoindenter**	**Resonance**
Ni	156.9GPa	156.7±5GPa	158.1±2GPa
Ni-diamond (avg. dia. 350 nm)	165.9GPa	164.0±5GPa	163.3±2GPa
Ni-diamond (avg. dia. 50 nm)	178.2GPa	178.0±5GPa	178.2±2GPa

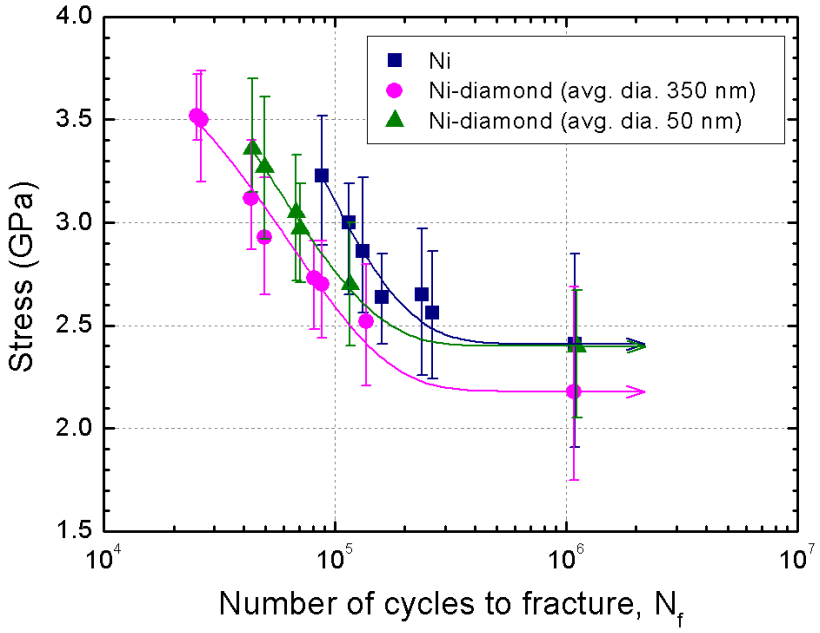

Fig. 6. *S-N* curve of microsized cantilever-beam specimens made of the electroplated Ni and Ni-diamond nanocomposites from the fatigue life tests.

3.3 Fatigue-lifetime test

As aforementioned in Section 2, the fatigue-lifetime test of the beams made of electroplated Ni and Ni-diamond composites are performed using a micro-probe

controlled by the test machine to cyclically apply a sinusoidal displacement on the free-end of cantilever beam with a frequency of 20Hz. Fatigue lifetime is obtained from different cyclic displacement loadings which are below δ_{max} for each fatigue test condition. Besides, all of the lifetime testes are performed in air and at room temperature. Fig. 6 shows the result of fatigue-lifetime tests in terms of *S*-*N* curve. The *S*-*N* curve, a plot of loading stress (*S*) versus the number of cycles to fracture (*N*) is generally utilized for presenting fatigue data. The values of stress amplitude used in the *S*-*N* curve are evaluated by FEA from the cyclic displacement loading, as shown in Fig. 7 [14, 15] at the root corner with the maximum stress. In the *S*-*N* curve of Fig. 6, each data point is determined while the specimen is broken as shown in Fig. 8, where the loading force detected by the load cell will become diminutive and the number of cycles to fracture will be recorded, simultaneously. In general, fatigue strength is defined as a stress value where the specimen has no failure after 10^6 cycles [16]. Therefore, as shown in Fig. 6, the fatigue strengths are obtained as 2.41GPa, 2.18GPa, and 2.40GPa for the electroplated Ni, the Ni-diamond nanocomposite incorporated with 350nm in diameter nano-diamond powders, and the one with 50nm in diameter nano-diamond powders, respectively. Meanwhile, it is found that the fatigue strength of Ni-diamond nanocomposite can have 10% increase with the reduction of nano-diamond particle size from 350nm to 50nm, and the fatigue lifetime of Ni-diamond nanocomposite with the average particle-diameter of 50nm would be the same as that of pure electroplated Ni in the low loading stress regime.

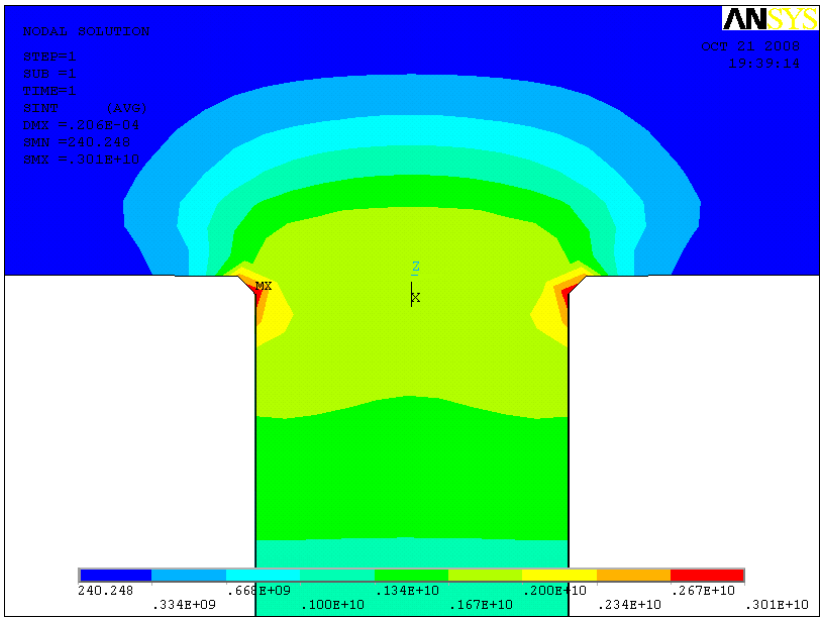

Fig. 7. FEA calculated stress-distribution of specimen under the cyclic displacement loading.

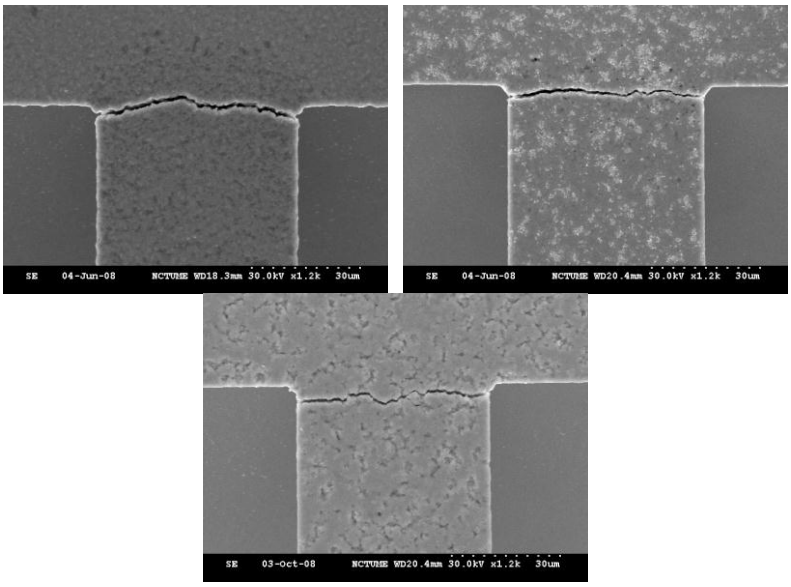

(a) (b) (c)

Fig. 8. SEM pictures of electroplated specimen appearance after fatigue fracture: (a) Ni; (b) Ni-diamond nanocomposite with average particle-diameter of 350nm; (c) Ni-diamond nanocomposite with average particle-diameter of 50nm.

4. Discussions

Fatigue of ductile material is generally attributed to cyclic plastic deformation involving dislocation motion. The motion would result in the alternating, blunting, re-sharpening, and advancing of a crack tip in a material [17]. From the FEA calculated stress distribution in Fig. 7, it can be found that the maximum stress value is concentrated at the root-corner of cantilever beam. Under cyclic stress loading, crack tip will occur initially at the stress-concentrated zone such as the root-corner of specimen, as shown in Fig. 9(a). Then, the cracks will grow from two ends of the root-corner of specimen (Fig. 9(b)). Finally, the beam will fracture as soon as two ends meet together (Fig. 9(c)). Fig. 10 shows the SEM picture of fatigue fracture interface of Ni-based beam. The cup-cone fracture morphology is a typical ductile characteristic of metal-based material. Fig. 6 has shown that electroplated Ni-diamond nanocomposites have slightly smaller fatigue lifetime than that of pure electroplated Ni especially for larger size particles. It can be attributed to the ductility reduction by incorporation of second-phase particles. As shown in Fig. 10(a) and 10(b) which are the fatigue fracture interface of the pure Ni and the Ni-diamond nanocomposite with the average particle-diameter of 350nm, respectively, the cup-cone has been become finer and the interface morphology has become toward to brittle fracture. In the nanocomposite system, nano-diamond is a source to generate dislocation but also a barrier to block dislocation motion because of the high

hardness of diamond. Due to aggravated multiplication and motion hindrance of dislocations in the composite system, crack and void would be easily formed and make the material become brittle. Thus, both the fatigue lifetime and strength of Ni-diamond nanocomposite will degrade and become worse than that of pure electroplated Ni.

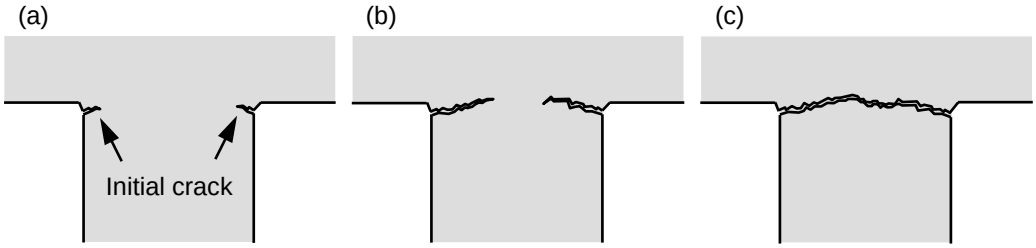

Fig. 9. Schematic process of fatigue fracture on microsized cantilever-beam specimen: (a) crack initiation; (b) crack growth; (c) specimen failure.

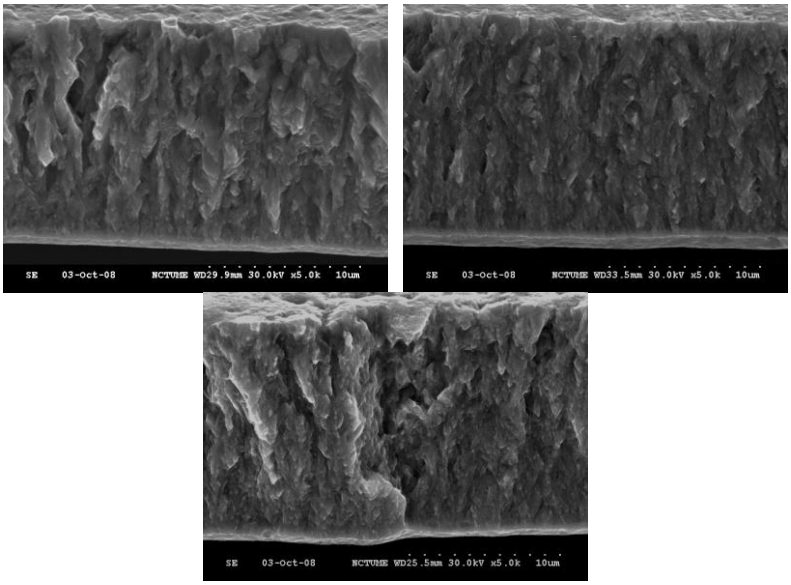

(a) (b) (c)

Fig. 10. SEM pictures of cross-sectional morphology of electroplated specimen after fatigue test (~3GPa stress amplitude): (a) Ni; (b) Ni-diamond nanocomposite with average particle-diameter of 350nm; (c) Ni-diamond nanocomposite with average particle-diameter of 50nm.

As aforementioned in Section 3.2, the electroplated Ni-diamond nanocomposites have higher Young's modulus values than that of pure electroplated Ni. Such improvement can be attributed to the particle reinforcement in matrix that the diamond has a larger Young's modulus (~1100GPa [18]) than that of pure

electroplated Ni (~156.7GPa as measured). According to the rule-of-mixtures equations [19, 20], the Young's modulus of the composite could be estimated as the one just falling between the upper and lower bounds as follows:
Upper bound based on the assumption that two phases in a composite are arranged in parallel,

$$E_{c,\text{parallel}} = E_m V_m + E_p V_p \quad (2)$$

and lower bound based on the assumption of two in-series phases,

$$E_{c,\text{series}} = \frac{E_m E_p}{E_m V_p + E_p V_m} \quad (3)$$

where E and V denote the Young's modulus and volume fraction, respectively, and the subscripts of c, m, and p represent composite, matrix, and particle phases. From Eq. (2) and (3), the calculated upper and lower bound values of Young's modulus are 157.2GPa and 160.0GPa for the electroplated Ni-diamond nanocomposites with the average particle-diameter of 350nm, and 157.3GPa and 160.6GPa for the composite one with the average particle-diameter of 50nm, respectively. Therefore, electroplated Ni-diamond nanocomposites will be expected to have a higher Young's modulus value based on the rule-of-mixtures. These calculated Young's modulus values are quite close to the values derived by different methods as listed in Table 2. Nevertheless, it is noted that, the Young's modulus of electroplated Ni-diamond nanocomposite with the average particle-diameter of 50nm has the largest value.

Previous researches [21-23] have observed that the decrease of particle size can have composite materials gain the largest strengthening and hardening effects which also result in the increases of fatigue lifetime and strength. Under the same volume fraction, more and more nano-particles will be introduced in the composite system with a decrease in the grain size of secondary phase. It could complicate the grain boundary system of the composite with different sliding systems which would hinder dislocation motion, make structure hardened, and prevent crack growth. In fact, the strengthening will be especially pronounced in the high cycle fatigue test with the low stress amplitude, as shown in Fig. 6. As the cyclic-loaded-stress amplitude being reduced, the fatigue lifetime of the electroplated Ni-diamond nanocomposite with small particle size of 50nm will approach gradually to the one of pure electroplated Ni. It is because small particle size means dislocations could still cut through or bypass the secondary phase under low cyclic loaded. The cutting through or by-passing behavior will make the fracture more behave like ductile even though the secondary

phase could effectively result in the multiplication and motion hindrance of dislocations. The fatigue lifetime and strength of the electroplated Ni-diamond nanocomposite can, therefore, be improved by incorporating small size particles. In fact, the tendency has also been founded in the fracture interfaces, as shown in Fig. 10(a) and 10(c). The cup-cone fracture morphology of Ni-diamond nanocomposite with the average particle-diameter of 50nm appears closely to that of pure electroplated Ni.

In addition, by comparing the Young's modulus values between Table 2 and rule-of-mixtures calculation, it can be found that the effect of particle size is remarkable for Young's modulus improvement with the particle size reduction of nano-diamonds [23]. The strengthening can also be well explained by aforementioned sliding system complication that makes Young's modulus of the Ni-based composite depend on not only volume fraction of nano-diamond particle but also its sizes.

5. Conclusions

Fatigue characterizations of electroplated Ni and Ni-diamond nanocomposite including Young's modulus, fatigue life, and fatigue strength, have been performed by employing bending test to microsized cantilever-beam specimens. Experimental results show that Ni-diamond nanocomposite has higher Young's modulus than that of pure electroplated Ni due to the particle reinforcement in matrix, but it has slightly shorter fatigue lifetime and weaker fatigue strength than that of pure electroplated Ni due to the ductility reduction resulted by the nano-diamonds. Nevertheless, once incorporated diamond particle size is reduced from 350nm to 50nm, the fatigue lifetime of Ni-diamond nanocomposite can be improved and its fatigue strength can be as strong as the pure electroplated Ni. These improvements of fatigue lifetime and strength can be attributed to the particle size effect. Under the same weight fraction, small diamond size means more diamond particles to complicate the composite grain boundary system which will hinder dislocation motion, make structure hardened, and prevent crack growth. Taking advantages of similar fatigue strength as pure Ni, low electroplating temperature (~50°C), and MEMS/CMOS compatible process, the electroplated Ni-diamond nanocomposite with enhanced Young's modulus is expected as an appropriate material for high frequency and moving components of MEMS devices.

References

[1] L.N. Tsai, G.R. Shen, Y.T. Cheng, W. Hsu, Performance improvement of an electrothermal microactuator fabricated using Ni-diamond nanocomposite, *J.*

Microelectromech. Syst. 15 (2006) pp. 149-158.

[2] L.N. Tsai, Y.T. Cheng, W. Hsu, Nanocomposite Effects on the of Thermal Expansion Modification for High Performance Electro-Thermal Microactuator, in: *Proceeding of IEEE MEMS'05*, Miami, Florida, U.S.A., 2005, pp. 467-470.

[3] Y.C. Lee, L.N. Tsai, Y.T. Cheng, W. Hsu, Performance enhancement of comb drive actuators utilizing electroplated nickel-diamond nanocomposite, in: *Proceeding of Asia-Pacific Conference of Transducers and Micro-Nano Technology (APCOT)*, Singapore, 2006.

[4] H.S. Cho, K.J. Hemker, K. Lian, J. Goettert, G. Dirras, Measured mechanical properties of LIGA Ni structures, *Sensors and actuators A* 103 (2003) pp. 59-63.

[5] D. Son, J. Kim, T.W. Lim, D. Kwon, Evaluation of fatigue strength of LIGA nickel film by microtensile tests, *Scr. Mater.* 50 (2004) pp. 1265-1269.

[6] T. Yi, C.J. Kim, Measurement of mechanical properties for MEMS materials, *Meas. Sci. Technol.* 10 (1999) pp. 706-716.

[7] S. Maekawa, K. Takashima, M. Shimojo, Y. Higo, S. Sugiura, B. Pfister, M.V. Swain, Fatigue Tests of Ni-P Amorphous Alloy Microcantilever Beams, *Jpn. J. Appl. Phys.* 38 (1999) pp. 7194-7198.

[8] S. Johansson, J.Å. Schweitz, L. Tenerz, J. Tirén, Fracture testing of silicon microelements in situ in a scanning electron microscope, *J. Appl. Phys.* 63 (1988) pp. 4799-4803.

[9] H.K. Liu, B.J. Lee, P.P. Liu, Low cycle fatigue of single crystal silicon thin films, *Sensors and Actuators A* 140 (2007) pp. 257-265.

[10] C.J. Wilson, A. Ormeggi, M. Narbutovskih, Fracture testing of silicon microcantilever beams, *J. Appl. Phys.* 79 (1996) pp. 2386-2393.

[11] C. Hsu, C. Tsou, W. Fang, Measuring thin film elastic modulus using a micromachined cantilever bending test by nanoindenter, *J. Micro/Nanolith. MEMS MOEMS* 6 (2007) pp. 033011.

[12] A.C. Fischer-Cripps, *Nanoindentation*, Springer, New York, 1st edn., 2002, pp. 27-30.

[13] L. Kiesewetter, J.M. Zhang, D. Houdeau, A. Steckenborn, Determination of Young's moduli of micromechanical thin films using the resonance method, *Sensors and Actuators A* 35 (1992) pp. 153-159.

[14] K.P. Larsen, A.A. Rasmussen, J.T. Ravnkilde, M. Ginnerup, O. Hansen, MEMS device for bending test measurements of fatigue and creep of electroplated nickel, *Sensors and Actuators A* 103 (2003) pp. 156-164.

[15] S.M. Allameh, P. Shrotriya, A. Butterwick, S.B. Brown, W.O. Soboyejo, Surface topography evolution and fatigue fracture in polysilicon MEMS structures, *J. Microelectromech. Syst.* 12 (2003) pp. 313-324.

[16] J.E. Shigley, C.R. Mischke, R.G. Budynas, *Mechanical Engineering Design*, Mc Graw Hill, New York, 7th ed., 2003, pp. 313-315.

[17] C.L. Muhlstein, E.A. Stach, R.O. Ritchie, Mechanism of fatigue in micron-scale films of polycrystalline silicon for microelectromechanical systems, *Appl. Phys. Lett.* 80 (2002) pp. 1532-1534.

[18] D. Schneider, M.D. Tucker, Non-destructive characterization and evaluation of thin films by laser-induced ultrasonic surface waves, *Thin Solid Films* 290-291 (1996) pp. 305-311.

[19] W.D. Callister Jr., *Materials Science and Engineering*, Wiley, New York, 4th edn., 1996, pp. 513.

[20] C.L. Hsieh, W.H. Tuan, Elastic and thermal expansion behavior of two-phase composites, *Mater. Sci. Eng. A* 425 (2006) pp. 349-360.

[21] Z. Xue, Y. Huang, M. Li, Particle size effect in metallic materials: a study by the theory of mechanism-based strain gradient plasticity, *Acta Mater.* 50 (2002) pp. 149-160.

[22] Q. Zhang, D.L. Chen, A model for predicting the particle size dependence of the low cycle fatigue life in discontinuously reinforced MMCs, *Scripta Mater.* 51 (2004) pp. 863-867.

[23] N. Chawla, C. Andres, J.W. Jones, J.E. Allison, Effect of SiC volume fraction and particle size on the fatigue resistance of a 2080 Al/SiC_p composite, *Metall. Mater. Trans. A* 29 (1998), pp. 2843-2854.

Part III

1. Introduction

As a micromechanical structural material, electroplated Ni has drawn many research attentions in MEMS manufacture since it has the characteristics of high deposition rate, low process temperature, low manufacture cost, good electrical conductivity and high mechanical strength very suitable for post-CMOS (Complementary Metal Oxide Semiconductor) MEMS fabrication [1, 2]. A variety of high performance Ni-based MEMS microactuators have been demonstrated, such as the electro-thermal actuators with large output displacement for low power applications [3,4] and the micromechanical resonators with high quality factor for monolithic RF CMOS oscillator fabrication [1,5]. Owing to the intrinsic ferromagnetic property of Ni, Ni-based MEMS devices can be also designed with a magnetic-force-driven function [6, 7], applicable for the use in highly conductive salty solutions, such as in-vivo biological systems [8]. Using the multiple molding/electroplating technology [9], 3-D Ni-based MEMS structures can be constructed with a high aspect ratio of the structural thickness to width (>100) which can effectively increase the sensitivity but also reduce the driving voltage in any capacitive type transducers [10, 11]. Recently, it has been found that

the physical properties of Ni can be further reinforced by incorporating a secondary material such as Al_2O_3, SiC, SiO_2, diamond and CNT (Carbon Nanotube) within itself [12-15]. Previously, we reported a simple process by adding diamond or CNT nanoparticles into an electroplating bath to fabricate Ni-based nanocomposite electrothermal microactuators [16, 17]. With appropriate incorporation of the secondary phase, such as diamond or CNT nanoparticles, the nanocomposite actuator can have superior performance including lower power consumption and larger output displacement due to the increase of Young's modulus, hardness and CTE (coefficient of thermal expansion) even without sacrificing its intrinsic mechanical reliability [16, 18]. The property enhancements have led such electroplated Ni-based nanocomposite films for more MEMS applications, especially in RF MEMS like the fabrication of MEMS switch, resonator and filter components.

Nevertheless, as-electroplated Ni film is usually accompanied with residual stress which would cause significant undesired structural deformation like beam curling and membrane winkling in suspended Ni-based MEMS devices. Because of the deformed structures, the Ni-based MEMS device must suffer either the problem of performance mismatch like capacitance mismatch [17, 18] or the problem of performance degradation while the device structure is made stiffer than the original design [19]. So far, it is still a critical research topic to solve the curling phenomenon in electroplated Ni structures for future MEMS applications. Compensation design based on the pre-characterization of Ni film to predict its residual stress level is a commonly used technique to resolve the issue [20]. Since residual stress problem would become more severe in the Ni-based nanocomposite film while the electroplated Ni film contains the residual stress [14], design flexibility would be limited and alternative approach to resolve the problem is still required.

In general, the residual stress of thin film can be expressed as follows [22],

$$\sigma(z) = \sum_{k=0}^{\infty} \sigma_k \left(\frac{z}{h/2} \right)^k \tag{1}$$

where $z \in (-h/2, h/2)$ is the coordinate across the film thickness. For simplicity, the high-order ($k > 2$) terms are neglected and the expression can be modified as follows,

$$\sigma(z) \approx \sigma_0 + \frac{\sigma_1}{h/2} z \tag{2}$$

In the expression, the residual stress can be divided into two types of stresses which are mean stress (σ_0) and gradient stress (σ_1) respectively. Basically, the curl phenomenon is caused by the existence of gradient stress in an as-electroplated Ni film. The mean stress in electroplated Ni film has been well studied and shown that it would be a function of plating temperature, current density, and additives of electrolyte [23-25]. On the contrary, the gradient has not been investigated systemically and only plating temperature was identified as a key process parameter to reduce it so far. High plating temperature can lead to the gradient

stress relaxation of the film during plating because Ni atoms can migrate to relaxed positions [26]. Nevertheless, the Ni film electroplated at high temperature (over 70℃) usually accompanies with a high thermal stress level and the inclusion of nonmetallic atoms in the film which would affect the material elastic properties [24].

Therefore, in the work, we will demonstrate Ni-diamond micromechanical resonators for the first time without noticeable structure deformation resulted by the residual gradient stress. According to the previous studies [27-29], it was found that the residual stress is strongly correlated with grain size. Since plating current density will affect the nucleation and grain growth of an electroplated Ni film, it can be utilized as a process parameter for the modification and reduction of the gradient stress. At first, current density effects on the gradient stresses of Ni and Ni-diamond nanocomposite films are characterized using micro cantilevers. An optimal plating process with the lowest gradient stress is then derived and utilized to fabricate Ni-based micromechanical resonators. At final, the property enhancement of the diamond-incorporated Ni composite film is verified by characterizing the frequency responses of micromechanical resonators.

2. Electroplating

In the work, sulfamate-based Ni electrolyte is chosen for electroplating due to low residual stress in film deposition. Ni film is dc (direct current) electroplated in the plating solution with the electrolyte comprising of nickel sulfamate of 400 g L^{-1}, boric acid of 40 g L^{-1}, nickel chloride of 3 g L^{-1}, and wetting agent of 5 g L^{-1}. On the other hand, diamond nano-particles with 125 nm in diameter (Microdiamant AG Co., Ltd.) are added into the solution for Ni-diamond nanocomposite electroplating. An aerating system is utilized to increase the diffusion of Ni ion and keep the diamond nano-particles well suspended in the electrolyte. The plating solution with a pH level of 4.1~4.3 is put in a tank stored in a water immersion system where the temperature is kept at 35℃. Before being placed into the plating bath, the device substrate is first dipped in a 5% sulfate acid water solution for 10sec and then rinsed in de-ionized water for 5 min.

3. Film gradient stress characterization

Figure 1 shows a Ni micromechanical resonator electroplated with the current density of 20 mA cm^{-2}. The 6μm-thick as-released structure is warped down severely. Ni-diamond nanocomposite resonator also exhibits similar behavior. As aforementioned, the electroplated Ni-based films are not in a stress-free state and the warpage is caused by the existence of gradient stress. A cantilever beam can be utilized to well explain the residual gradient stress effect as shown in figure 2. Mean and gradient stresses will be generally formed in the cantilever beam while fabricated. When the layer underneath the cantilever is removed, the mean stress (σ_0) will be released and the gradient stress (σ_1) will make the beam

curled either upward (positive) or downward (negative). For our case, both Ni and Ni-diamond nanocomposites are subjected to a negative gradient stress.

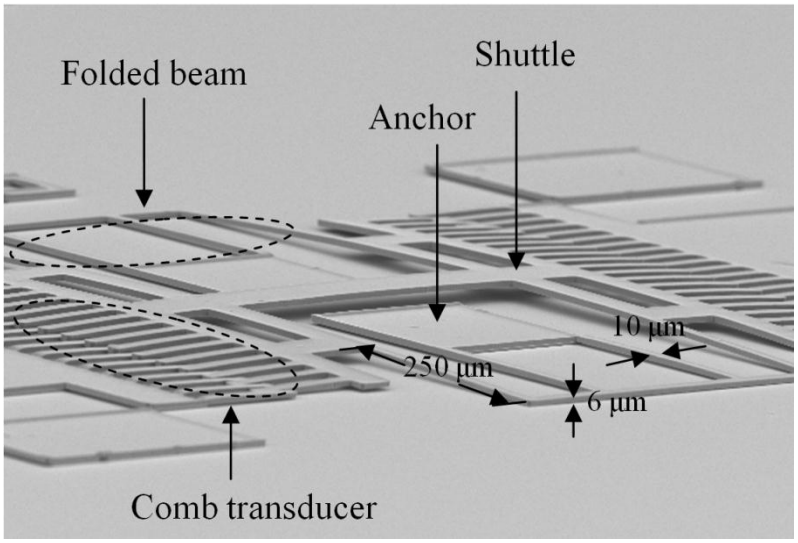

Figure 1. SEM photograph of Ni (comb-driven) micromechanical resonator with high gradient stress.

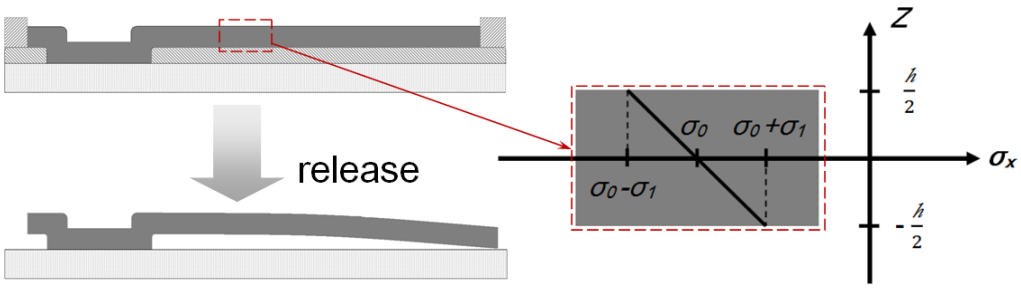

Figure 2. The states of cantilever beam before and after structural release (both Ni/Ni-diamond nanocomposite cantilever beams tend to warp downward).

The stress gradient, Γ, can be approximately estimated in a linear distribution and expressed as follows [21, 22, 30],

$$\Gamma = \frac{\Delta\sigma}{h} = \frac{2\sigma_1}{h} = \left(\frac{E}{1-\nu}\right)\frac{1}{\rho} \tag{3}$$

E and *v* are the Young's modulus and Poisson ratio of Ni film, respectively, and ρ is the radius of beam curvature. Thus, the surface profile and the curvature of cantilever will be measured by White-Light-Interferometer (FOGALE nanotech Inc.) and used for the characterization of the gradient stress of the electroplated Ni and Ni-diamond nanocomposite films.

4. Fabrication process

Figure 3 shows a typical process flow for MEMS fabrication using electroplated Ni or Ni-diamond nanocomposite. The fabrication starts with photoresist (PR) spin-coating and lithographically patterning on an electrical isolation layer, 500 nm thick SiO_2, followed by Ti/Ni layer (20/200 nm) deposition for device electrode fabrication on a silicon substrate (Fig. 3(a)). Sacrificial layer, like PR, is then coated, defined, and deposited with a sputtered Cu seed layer (200 nm) for following Ni-based composite electroplating (Fig. 3(b)). Before electroplating, thick PR like AZ-10XT is spun and patterned on the substrate as a mold (10 μm) where Ni-based film (6 μm) is electroplated to form microstructure (Fig. 3(c)). Device fabrication is then finished after the removal of PR mold, Cu seed layer, and sacrificial layer by acetone, the mixture of NH_4OH and H_2O_2, and PR stripper, respectively (Fig. 3(d)). For the case of cantilever beam, there is no need to fabricate the electrode underneath the beam for the curvature measurement, so the process steps of Ti/Ni layer (20/200 nm) deposition and patterning are skipped.

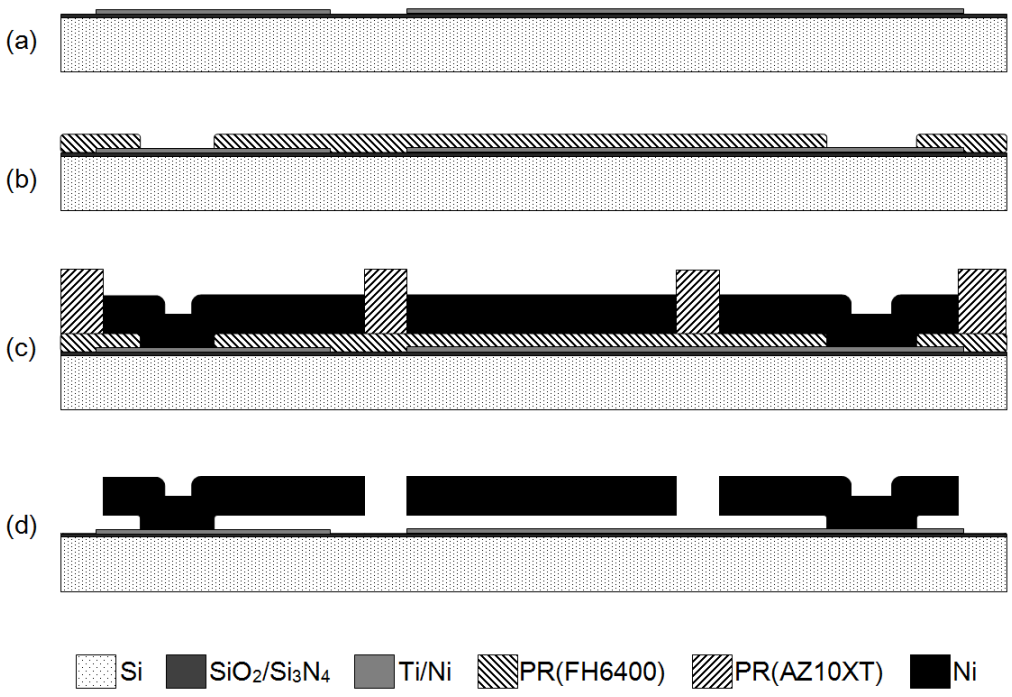

Figure 3. Fabrication flow chart (a) Ti/Ni electrode definition, (b) PR (FH6400) sacrificial layer and Cu seed layer deposition, (c) PR (AZ-10XT) mold and composite film electroplating, and (d) structure release.

5. Characterization setup of micro resonators

In the work, comb-driven resonator is utilized to demonstrate the optimal process with gradient stress reduction and the resonant frequency enhancement based on the improvement of Young's modulus/density ratio [18]. Figure 4 shows the experimental setup where MEMS Motion Analyzer (Etec Inc., MMA G2) is used for characterizing the resonant frequency of

resonators as shown in Fig. 4(a). The MMA combines microscopy and stroboscopic illumination to analyze the periodical motions of microstructures. The resonator is driven by the function generator of the MMA. The V_{bias} (from 60 to 120 V) and V_i (from 2 to 10 V) are applied on the resonating structure and fix comb-electrode part respectively as shown in Fig. 4(b) and the motion images at different frequency can be captured by the optical system of the MMA. Inset pictures 1-3 show the relative motion of comb-fingers on the resonator in the state of released, middle stroked, and pulled, respectively, as shown in Fig. 4(c). According to the image data captured at different frequency, the frequency response of the μ-resonator with different vibrating amplitude can be obtained.

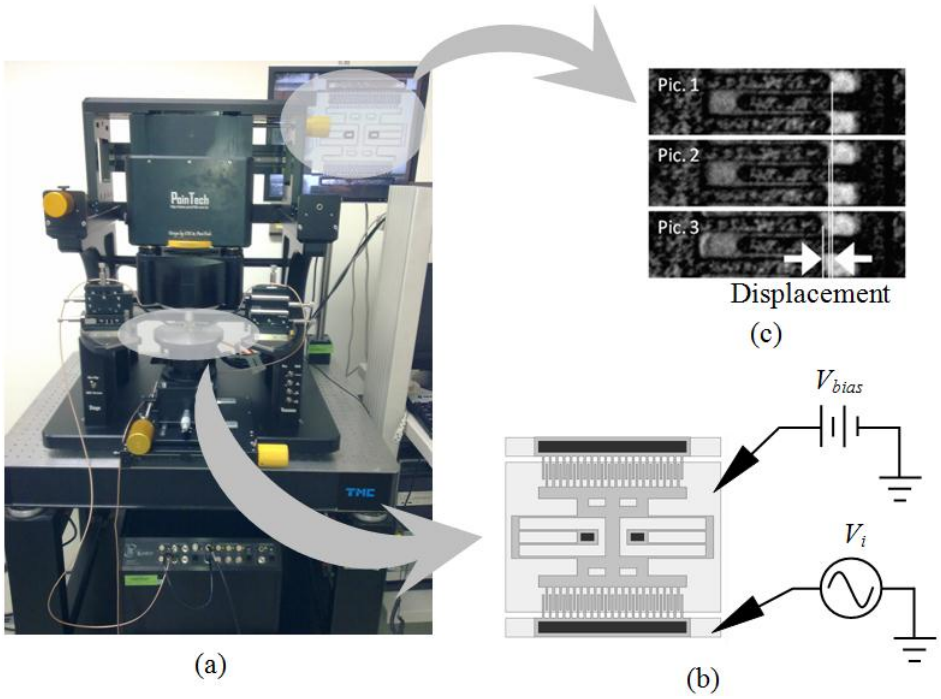

Figure 4. The measurement setup. (a)MEMS motion analyzer. (b) Comb resonator is electric driven and the response is measured by (c) optical motion analysis system.

6. Results and Discussion

Figure 5 shows the relation between plating current versus the stress gradient and deposition rate of electroplated Ni and Ni-diamond nanocomposite films. Although the deposition rate of Ni and Ni-diamond nanocomposite film increases with the increase of plating current density, it is inevitable to have a warped structure plated with high current density owing to large gradient stress. In addition, Ni-diamond nanocomposite film has higher gradient stress than the Ni one. For the same current density, the gradient stress of Ni-diamond nanocomposite film is about 1.3 times larger than that of Ni film. By lowering plating current density form 15.3 to 0.8 mA cm^{-2}, the stress gradient can have 45% and 27% reduction for Ni and Ni-diamond nanocomposite respectively.

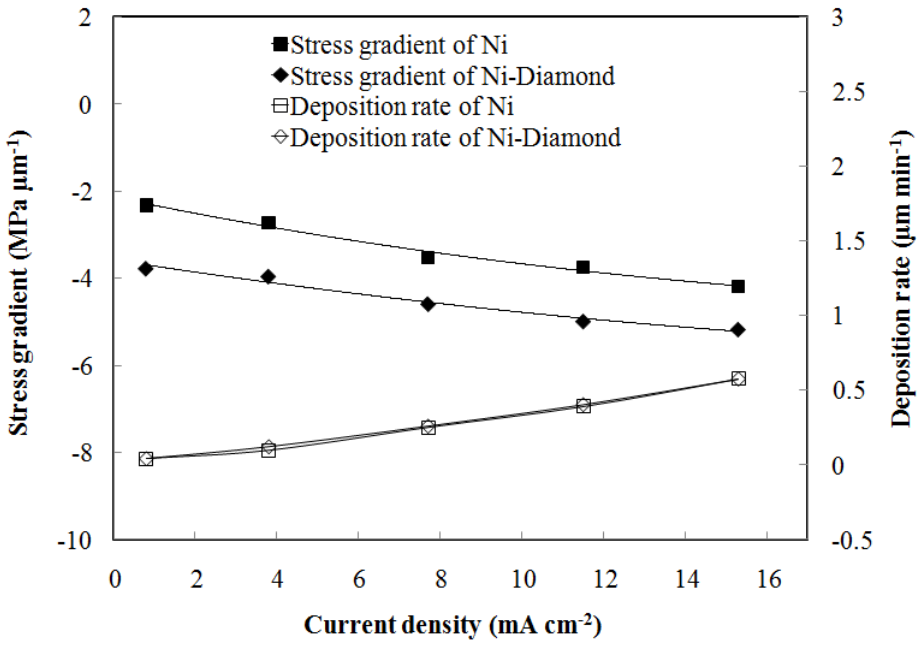

Figure 5. The stress gradient and deposition rate of Ni and Ni-diamond nanocomposite film under different electroplating current density.

From the cross sectional images taken by focused ion beam (FIB) as shown in Fig. 6, it is found that the Ni film plated with higher current density is comprised of finer grains. Similar phenomenon has been found in several literatures [29, 31-33]. In general, the grain structures in a polycrystalline film would gradually evolve from a microstructure similar to the nucleation/seed layer to a texture with a preferred growth direction and the evolution would accompany with the variation of grain size and residual stress distribution [27-29]. In other words, a stress gradient would form in a polycrystalline film while the grain evolution takes place. From the FIB images, it is found that the film plated with higher current density will have more drastic grain size variation. In Fig. 6(a), the average grain size of the Ni film plated with 15.3 mA cm^{-2} is small and then becomes larger form the bottom layer to top surface. On the contrary, the average grain size of the Ni film plated with 0.8 mA cm^{-2} as shown in Fig. 6(b) is larger than the previous one but its grain size variation is not drastic. Similar phenomenon has been observed in the nanocomposite films. In Fig. 6(c), the composite film plated with 0.8 mA cm^{-2} has a grain size distribution similar to the Ni film even though diamond nanoparticles are incorporated.

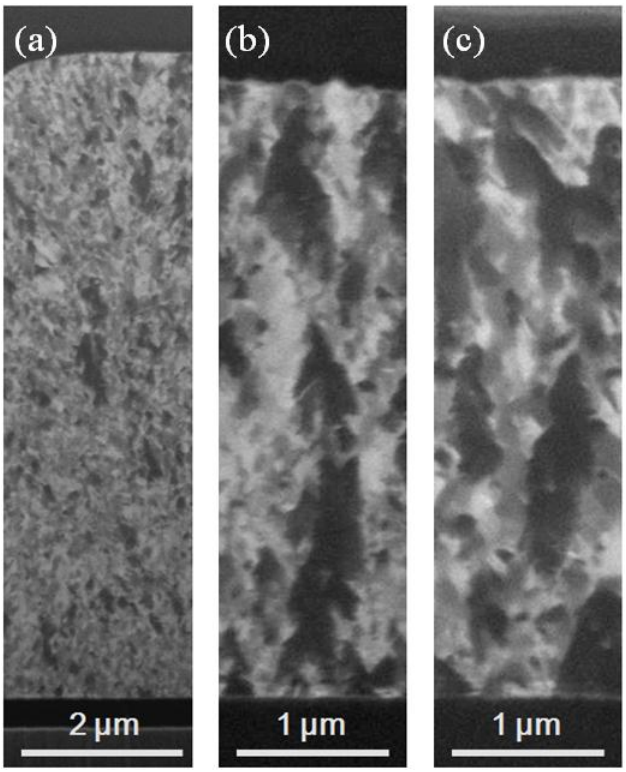

Figure 6. FIB cross sectional images of Ni films electroplated at (a) 15.3 mA cm^{-2} and (b) 0.8 mA cm^{-2} and (c) Ni-diamond at 0.8 mA cm^{-2}.

The origin of the gradient stress can be further illustrated by the grain boundary relaxation model [27-29]. The residual stress is induced by the physical energy difference between the surface energy and the grain boundary energy in grain growth [27],

$$\sigma(z) = \frac{\delta}{G(z)}\left(\frac{E}{1-\nu}\right) \tag{4}$$

δ and G(z) are the shrinkage of the grain boundary and the grain size respectively. In our case, the electroplated Ni plated with a high current density condition exhibits the non-uniform grain size distribution as aforementioned. The stresses in the electroplated Ni film would, therefore, decrease when the film gets thicker and the film would tend to form warpage. Considering a thin film with the thickness of h, the stress gradient (Γ) of the film can be derived and expressed as follows by substituting (4) into (3),

$$\Gamma = \frac{\Delta\sigma}{h} = -\frac{\delta E}{1-\nu}\cdot\frac{\Delta G}{h}\cdot\frac{1}{G(z_1)G(z_0)} \tag{5}$$

where z_0 and z_1 are the location at the bottom and top surface of the film, respectively. In this expression, it shows the correlation of gradient stress with the grain size variation (ΔG) and grain size ($G(z)$). With lower plating current density, the film can have larger and uniformly distributed grain size which can effectively result in a lower gradient stress. Figure 7 shows the SEM photographs of Ni (Fig. 7(a)) and Ni-diamond nanocomposite resonators (Fig. 7(b)) electroplated at 0.8 mA cm^{-2}. There is indeed no noticeable warpage

happening in both resonators.

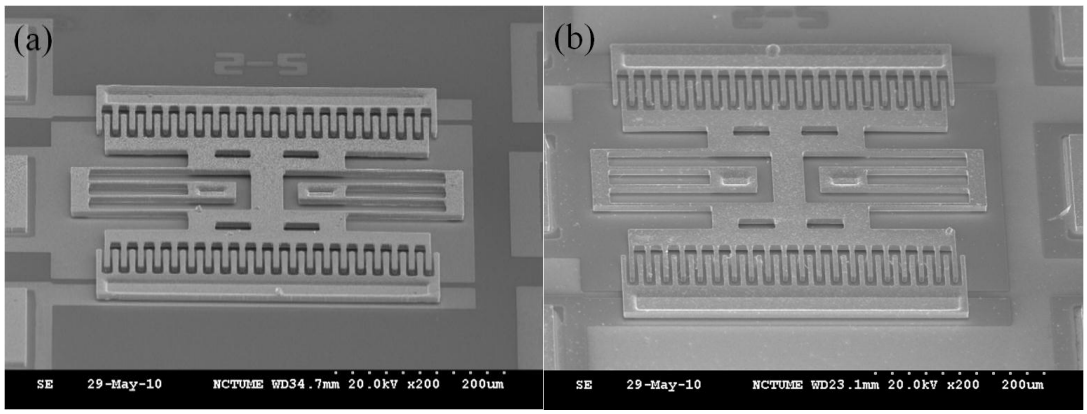

Figure 7. SEM photographs of (a) Ni and (b) Ni-diamond nanocomposite resonators after stress modification.

Figure 8 shows the frequency response of the resonators made of Ni and Ni-diamond nanocomposite indicating the related resonant frequencies are 22.55 and 25.75 kHz respectively. About 14% resonant frequency enhancement can be realized in the Ni-diamond nanocomposite resonator where the composite film is electroplated in a Ni solution with 2g L^{-1} diamond nanoparticles. Meanwhile, the measured response also shows the Ni-diamond resonator has a higher quality factor than that of Ni at atmospheric pressure. The frequency enhancement can be expected based on the elemental analysis of electroplated nanocomposite film using the tool of elemental analyzer (Heraeus, varioIII-NCH) as shown in figure 9. From the detected C concentration, it is found that the volume percentage of incorporated diamond is proportion to the diamond concentration in the Ni plating bath. For the nanocomposite film plated in the bath with 2g L^{-1} diamond nanoparticles, the volume percentage of the incorporated diamond can be increased to 0.46%. According to rule of mixture, the Young's modulus of two-phase composite can be estimated by the following expression [34],

$$E_{composite} = E_A V_A + E_B V_B \quad (6)$$

where the E and V are Young's modulus and volume fraction of the matrix and secondary phase, respectively. The mechanical property of Ni film with diamond volume ratio of 0.46% can only have 2.7% Young's modulus enhancement which indicates only 1.7% resonant frequency increase can be achieved. Comparing with the measured resonant frequency of the resonator, nano-diamond incorporation can bring more resonant frequency enhancement than that estimated by rule of mixture. The frequency enhancement can be attributed to two possible factors which can result in the Young's modulus increase of the nanocomposite film. According to the previous study [35], it was found that the more compressive-stressed film will come with a higher Young's modulus. Since the diamond incorporation would cause Ni film with more

compressive stress [14], it may cause the increase of Ni Young's modulus so that the Young's modulus of the nanocomposite can be enhanced. Meanwhile, the resonant frequency enhancement can be possibly attributed to more nano-diamond incorporation in the supporting beams of the comb-driven resonators due to limited beam width. Further investigation regarding the stress effect on the mechanical property change in the Ni matrix and the geometrical effect of plating mold on the incorporation of nano-diamond in the composite film are, therefore, required for potential MEMS applications.

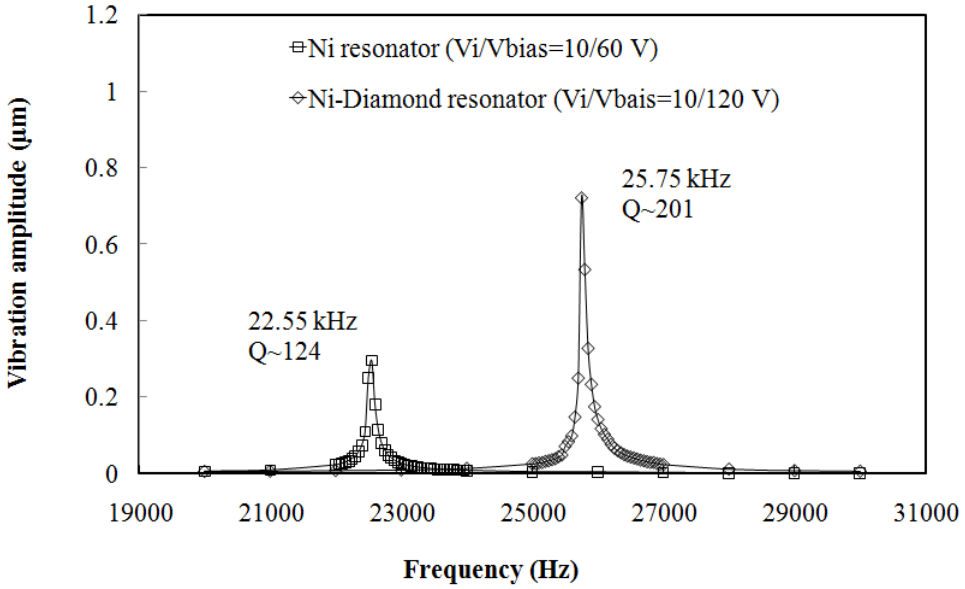

Figure 8. Frequency responses of Ni and Ni-diamond nancomposite comb resonators at atmospheric pressure.

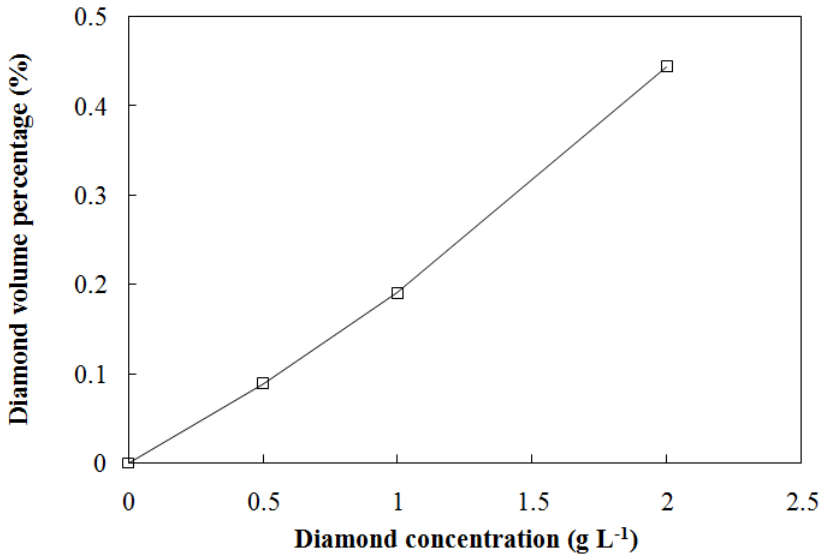

Figure 9. Incorporated diamond volume percentage in the nanocomposite with different diamond concentrations in electrolyte.

7. Conclusion

Gradient stress reduction by lowering plating current can effectively prevent the structural warpage of as-fabricated MEMS device owing to the formation of larger Ni grains uniformly distributed in the electroplated Ni-based films. Experimental results indicate about 45% and 27% reduction of the gradient stress can be achieved in Ni and Ni-diamond nanocomposite film by reducing the plating current density from 15.3 to 0.8 mA cm^{-2}. The stress reduction is the key to successfully fabricate electroplated Ni-diamond nanocomposite comb-driven microresonators. In this work, the nanocomposite resonator has shown better device performance including the increase of resonant frequency and quality factor in comparison with the same type of resonator made of electroplated Ni. About 14% resonant frequency enhancement has been found in the nanocomposite resonator made of the Ni-diamond nanocomposite plated in the bath containing 2 g L^{-1} nano diamond particles with 125 nm in diameter. The enhancement can be attributed to the increase of Young's modulus/density ratio via the incorporation of diamond nanoparticles in the Ni matrix.

References

[1] Huang W-L, Ren Z, Lin Y-W, Chen H-Y, Lahann J and Nguyen C T-C 2008 Fully monolithic CMOS nickel micromechanical resonator oscillator *Proc.IEEE Int. Conf. Micro Electro Mech. Syst.* (Tucson, AZ) 10-13

[2] Alper S E, Silay K M and Akin T 2006 A low-cost rate-grade nickel microgyroscope, *Sensors and Actuators* A **132** 171-181

[3] Hsu C P and Hsu W 2006 Design and characterization of an electrothermally driven monolithic long-stretch microdrive in compact arrangement *J. Microelectromech. Syst.* **15** 935-944

[4] Girbau D, Pradell L, Lazaro A and Nebot A 2007 Electrothermally actuated RF MEMS switches suspended on a low-resistivity substrate *J. Microelectromech. Syst.* **16** 1061-1070

[5] Huang W-L, Ren Z and Nguyen C T-C 2006 Nickel vibrating micromechanical disk resonator with solid dielectric capacitive-transducer gap *Proc., IEEE Freq. Ctrl. Symp.* (Miami, FL) 839-847

[6] Vasquez D J and Judy J W 2008 Flexure-based nanomagnetic actuators and their ultimate scaling limits *Proc. IEEE Int. Conf. MEMS* (Tucson, AZ) 737-741

[7] Chang C W and Hsu W 2009 Three-dimensional micro assembly of a hinged nickel micro device by magnetic lifting and micro resistance welding *J. Micromech. Microeng.* **19** 105026

[8] Lee S A, Bergsneider M and Judy J W 2007 Magnetic microactuators for MEMS-enabled ventricular catheters for hydrocephalus *Proc. of the 3rd Int. Conf. IEEE Engineering in*

Medicine and Biology Society Conference on Neural Engineering (Kohala Coast, HI) 65-68

[9] Cohen A, Zhang G, Tseng F G, Frodis U, Mansfeld F and Will P 1999 EFAB: rapid, low-cost desktop micromachining of high aspect ratio true 3-D MEMS *Proc.IEEE Int. Conf. Micro Electro Mech. Syst.* 244–251.

[10] Kataoka K, Itoh T, Suga T and Inoue K 2004 Contact properties of Ni micro-springs for MEMS probe card *Proc. 50th IEEE Holm Conf. Elect. Contacts* 231-235

[11] Alper S E, Ocak I E and Akin T 2007 Ultrathick and high-aspect-ratio nickel microgyroscope using EFAB multilayer additive electroforming *J. Microelectromech. Syst.* **16** 1025-1035

[12] Kuo S L, Chen Y C, Ger M D and Hwu W H 2004 Nano-particles dispersion effect on Ni/Al2O3 composite coatings *Materials Chemistry and Physics* **86** 5–10

[13] Orlovskaja L, Periene N, Kurtinaitiene M and Surviliene S 1999 Ni–SiC composite plated under a modulated current, *Surface and Coatings Technology* **111** 234–239

[14] Teh K S, Cheng Y-T and Lin L 2005 MEMS fabrication based on nickel-nanocomposite: film deposition and characterization *J. Micromech. Microeng.* **15** 2205–2215

[15] Chao T-Y, Shen G-R and Cheng Y-T 2006 Comparative study of Ni–P–diamond and Ni–P–CNT nanocomposite films *J. Electrochem. Soc.* **153** G98-G104

[16] Tsai L-N, Cheng Y T, Hsu W and Fang W 2006 Ni-carbon nanotubes nanocomposite for robust microelectromechanical systems fabrication *J. Vac. Sci. Tech.***24** 205-210

[17] Huang C-S, Chung J, Cheng Y-T and Hsu W 2009 Investigation of Ni-based thermal bimaterial structure for sensor and actuator application *Sensors and Actuators* A **149** 298-304

[18] Tsai L-N, Shen G-R, Cheng Y-T and Hsu W 2006 Performance improvement of an electrothermal microactuator fabricated using Ni-diamond nanocomposite, *J. Microelectromech. Syst.* **15** 149-158

[19] Pacheco S P, Katehi L P B and Nguyen C T-C 2000 Design of low actuation voltage RF MEMS switch *IEEE MTT-S Int. Microwave Symp. Dig.* **1** 165-168

[20] Peroulis D, Pacheco S, Sarabandi K and Katehi L P B 2001 Alleviating the adverse stress effects of residual stress in RF MEMS switches *Proc. Eur. Microwave Conf.* **1** 173-176

[21] Hea S, Chang J S, Li L and Ho H 2009 Characterization of Young's modulus and residual stress gradient of MetalMUMPs electroplated nickel film *Sensors and Actuators* A **154** 149–156.

[22] Fang W and Wickert J A 1996 Determining mean and gradient residual stresses in thin films using micromachined cantilevers *J. Micromech. Microeng.* **6** 301–309

[23] Hearne S J and Floro J A 2005 Mechanisms inducing compressive stress during electrodeposition of Ni *J. Appl. Phys.* **97** 014901

[24] Luo J K, Pritschow M, Flewitt A J, Spearing S M, Fleck N A and Milne W I 2006 Effect

of process conditions on properties of electroplated Ni thin film for microsystem applications *J. Electrochem. Soc.* **153** D155-D161

[25] Tsuru Y, Nomura M and Foulkes F R 2000 Effects of chloride, bromide and iodide ions on internal stress in films deposited during high speed nickel electroplating from a nickel sulfamate bath *J. Appl. Electrochem.* **30** 231-238

[26] Luo J, He J H, Flewitt A, Moore D F, Spearing S M, Fleck N A and Milne W I 2005 Development of all metal electrothermal actuator and its applications *J. Microlithogr. Microfabr. Microsyst.* **4** 023012

[27] Hoffman R W 1976 Stresses in thin films: The relevance of grain boundaries and impurities *Thin Solid Films* **34** 185-190

[28] Nix W D and Clemens B M 1999 Crystallite coalescence: A mechanism for intrinsic tensile stresses in thin films *J. Mater. Res.* **14** 3467-3473

[29] Saitou M, Oshiro S and Sagawa Y 2008 Scaling behavior of internal stress in electrodeposited nickel thin films *J. Appl. Phys.* **104** 093518

[30] Ericson F, Greek S, Söderkvist J and Schweitz J Å 1997 High-sensitivity surface micromachined structures for internal stress and stress gradient evaluation *J. Micromech. Microeng.* **7** 30–36.

[31] Rashidi A M and Amadeh A 2010 Effect of electroplating parameters on microstructure of nanocrystalline nickel coatings *J. Mater. Sci. Technol.* **26** 82-86

[32] Wang L, Gao Y, Xu T and Xue Q 2006 A comparative study on the tribological behavior of nanocrystalline nickel and cobalt coatings correlated with grain size and phase structure *Materials Chemistry and Physics* **99** 96–103

[33] Rashidi A M and Amadeh A 2008 The effect of current density on the grain size of electrodeposited nanocrystalline nickel coatings *Surface & Coatings Technology* **202** 3772–3776

[34] Hsieh C-L and Tuan W-H 2006 Elastic and thermal expansion behavior of two-phase composites *Materials Science and Engineering* A **425** 349–360

[35] Woo Y and Kim S-H 2011 Sensitivity analysis of plating conditions on mechanical properties of thin film for MEMS applications *J. Mater. Sci. Technol.* **25** 1017-1022